



# A Simplified Mix Design for GGBS–Dolomite Geopolymer Concrete Using the Taguchi Method

P. K. Arjun Raj<sup>1</sup> · D. Sarath<sup>1</sup> · Praveen Nagarajan<sup>1</sup> · Blessen Skariah Thomas<sup>1</sup>

Received: 8 August 2023 / Accepted: 8 January 2024 / Published online: 8 February 2024  
© The Author(s), under exclusive licence to Shiraz University 2024

## Abstract

Incorporating industrial by-products into the manufacturing of geopolymer concrete has the potential to make concrete production more environmentally sustainable. This research employs ground granulated blast furnace slag (GGBS) and dolomite as aluminosilicate base materials, and sodium hydroxide solution (NaOH) and sodium silicate solution ( $\text{Na}_2\text{SiO}_3$ ) as the alkaline activators. The use of geopolymer concrete (GPC) allows for numerous design variables, which necessitates multiple trial experiments to determine an optimal GPC mix that achieves the desired strength. Therefore, the lack of a well-defined mix design process represents a notable obstacle to the industrial application of geopolymer concrete. In this study, the Taguchi approach is employed to optimize the mix design factors within the geopolymer concrete mixture, with a specific focus on achieving the desired strength criteria. The study includes a slump test, compressive strength test, and split tensile strength tests. The results of the tests match the target strength values, leading to the formulation of a mix design for GPC according to the Taguchi method, eliminating the need for extensive trials. The microstructure assessment of the mixtures, conducted through scanning electron microscopy (SEM), unveiled a more compact microstructure in the optimal blend. The  $\text{CO}_2$  assessment of GGBS–dolomite GPC highlighted a significant decrease in  $\text{CO}_2$  emissions when compared to an equivalent-grade normal concrete.

**Keywords** Geopolymer concrete · Dolomite · Taguchi method · Slump test · Compressive strength · Split tensile strength

## 1 Introduction

Geopolymer concrete (GPC), a novel construction material, has become increasingly popular nowadays. GPC has better strength and durability compared to conventional concrete (Saranya et al. 2019a). Further investigation is still required in the field of GPC because there is currently no standard technique for mix design (Li et al. 2019). The mix design for GPC is challenging because it depends on numerous factors like the proportion of Al and Si in the components, the alkali-to-binder ratio, the molarity of NaOH (sodium hydroxide), its ratio to  $\text{Na}_2\text{SiO}_3$  (sodium silicate), and the condition of curing (Saranya et al. 2019a); (Hadi et al. 2019); (Arthur et al. 2020); (Duxson et al. 2007). The mix design of geopolymer is also affected by the type of chemical constituents of binders and also the percentages of these

constituents. Unlike the mix design of conventional concrete, the GPC mix design demands many trials to obtain an accurate response of strength and durability due to many design variables. A simplified mix proportioning of GPC is essential because it reduces the time, energy, and effort needed. The Taguchi method is an optimization approach that has been successfully employed in the mix design of cement-based concretes (Türkmen et al. 2003). This method is employed in the present study to determine the optimum design mix for GPC by considering all the significant factors that influence strength and workability under ambient curing conditions. The Taguchi method and the guidelines of IS: 10,262–2019 are utilized to determine the optimum mix design variables of GPC.

Several early studies investigate the formulations and characteristics of geopolymer binder and concrete (Shi et al. 2011); (Garcia-Lodeiro et al. 2016); (García-Lodeiro et al. 2013). Cement manufacture is necessary for the construction of infrastructure. Cement production causes  $\text{CO}_2$  emission, which is harmful to the environment and causes global warming. GPC replaces cement with metakaolin, fly

✉ P. K. Arjun Raj  
arjunraj\_p200045ce@nitc.ac.in

<sup>1</sup> Department of Civil Engineering, National Institute of Technology Calicut, Kozhikode, Kerala 673601, India

ash, rice husk ash (Mareya et al. 2023), and GGBS (ground granulated blast furnace slag. Metakaolin-based geopolymer concrete has high strength and low durability (Marín-López et al. 2009); (Obeng et al. 2023). High-strength geopolymer concrete is produced by combining GGBS with fly ash and ordinary Portland cement (OPC) (Nath and Sarker 2014); (Salih et al. 2015). The most often utilized material for the development of a single aluminosilicate base material-based GPC is fly ash (Detphan and Chindaprasirt 2009); (Ahmad Dar and Azam 2015); (Pavithra et al. 2016); (Lekshmi and Sudhakumar 2022) (Sajan et al. 2021), which is a waste material obtained from coal-powered power plants (Nath and Sarker 2014). GGBS and fly ash can be combined to make high-strength ambient cured geopolymer concrete.

In the geopolymerization process, aluminosilicate materials undergo dissolution in an alkali solution, resulting in the formation of free  $\text{SiO}_4$  and  $\text{AlO}_4$  tetrahedral units (Davidovits 1989). Moreover, these  $\text{SiO}_4$  and  $\text{AlO}_4$  tetrahedra are interconnected in an alternating fashion, with charge-balancing cations supplied by alkali metal cations. This results in the generation of polymeric precursors such as  $-\text{SiO}_4-\text{AlO}_4-$ , or  $-\text{SiO}_4-\text{AlO}_4-\text{SiO}_4-$ , or  $-\text{SiO}_4-\text{AlO}_4-\text{SiO}_4-\text{SiO}_4-$ . The sharing of all oxygen atoms between two tetrahedral units facilitates the formation of monolithic geopolymer products (Khale and Chaudhary 2007).

GGBS is obtained as a by-product from the steel industry and has a similar chemical composition to cement. Approximately 0.45–0.50 tonnes of blast furnace slag will be produced per tonne of steel (Saranya et al. 2020). In the presence of alkali activators, GGBS will generate high-strength geopolymer concrete. In addition to early strength attainment, using GGBS to produce geopolymers lowers construction costs and eliminates issues related to its disposal.

Dolomite is a waste of rock-crushing plants, and its application in self-compacting concrete has been reported earlier (Barbhuiya 2011). According to reports, India accounted for 28% of global dolomite production (Chhattisgarh). Studies dealing with the effect of dolomite in GGBS geopolymer concrete are scarce. Dolomite is characterized by a significant composition of calcium oxide (CaO) and magnesium oxide (MgO). Furthermore, it also contains silicon dioxide ( $\text{SiO}_2$ ) and alumina oxide ( $\text{Al}_2\text{O}_3$ ). Notably, the presence of silica and alumina in dolomite makes it a potential raw material for geopolymer production. It also contributes to the rapid attainment of high strength in a very short period. According to a study by Yip et al. (2008), adding 20% dolomite to metakaolin increased the compressive strength of every sample tested. The strength exhibited a substantial increase, reaching a value exceeding 50 MPa during a period of 100 days. In a recent investigation by Nazar et al. (2023f), Nazar et al. (2023a), it was observed that the incorporation of additives such as multi-walled carbon nanotubes

(MWCNTs) led to enhanced mechanical properties in geopolymer composites, resulting in increased density. The study reported a notable maximum improvement of 14% in compressive strength when 0.3% MWCNTs were introduced into alkali-activated binders. Like dolomite, lime can also serve as a viable material for incorporation as a binding agent in geopolymer concrete, contributing calcium-rich elements to the mix (Nazar et al. 2023d).

In this study, GGBS and dolomite were blended to produce a novel geopolymer concrete. Early studies found that external heat is necessary to generate the polymerization process. But many researchers have tried to reduce the requirement of this heat treatment. For example, in the combination of fly ash and GGBS, due to CaO, GGBS can quicken the polymerization process and generate heat (Deb et al. 2014). Slag, on the other hand, considerably reduces the concrete's workability and curing time. According to research studies, the addition of GGBS decreases the mix's workability and reduces the GPC's setting time (Al-majidi et al. 2017). A properly proportioned mix of GGBS and dolomite has proven to be an excellent binder combination with an improved microstructure (Saranya et al. 2019a). The replacement of GGBS by dolomite helps to develop a GPC with a denser matrix and lesser pores. The mix becomes more workable as the percentage of dolomite in the mixture increases. The workability of GPC is increased by the large surface area of dolomite (Saranya et al. 2019a). The primary reasons that geopolymer concrete is not used more frequently are the lack of a standardized mix design process, poor workability, and high-temperature requirements for curing. Due to the brittle nature of GPC, their extensive use is limited by their poor performance when subjected to flexural and tensile loads. Nazar et al. (2023b) conducted a study indicating that the compressive and flexural strength rose with higher polypropylene (PP) and polyvinyl alcohol (PVA) fibre content. The mix with a fibre content equivalent to 1.5% of the binder exhibited the highest compressive strength at 46.95 MPa and flexural strength at 7.9 MPa. The mix design was carried out by several researchers using ACI guidelines (Cao et al. 2018). Numerous variables, including the ratio between alkali and binder, the ratio  $\text{Na}_2\text{SiO}_3/\text{NaOH}$ , the sodium hydroxide molarity, the superplasticizer dosage, the proportion of the binder, etc., affect the mix design of GPC. So enormous trials are required to develop a systematic mix design methodology for geopolymer concrete. Zheng et al. (2023), Nazar et al. (2023g), Nazar et al. (2023c) utilized gene expression programming (GEP) and multi-expression programming (MEP) to assess the compressive strength of alkali-activated materials. The objective was to compare these methods and establish more robust prediction models based on genetic algorithms. These methods face a limitation in that they

necessitate a substantial volume of dependable data to effectively operate (Nakkeeran et al. 2023); (Nazar et al. 2023e); (Nazar et al. 2022). The production process of geopolymer concrete is depicted in Fig. 1.

A statistical approach suggested by Japanese scientist Genichi Taguchi, generally recognized as the Taguchi technique (Galí et al. 2001), can be used to address these issues. Few works use this methodology for mix design (Dave et al. 2021); (Dave and Bhogayata 2020); (Onyia et al. 2022). The variables and the levels chosen are based on a significant number of trials, and the mix proportions used in this paper are for M45-grade geopolymer concrete.

The Taguchi approach is frequently applied in engineering; however, its use with geopolymer concrete is rather limited (Jithendra and Elavenil 2020); (Hadi et al. 2017). Since multiple factors influence mix design, this method does not account for the specific gravity, water absorption of coarse and fine natural aggregates, binders, and the zone of sand but instead incorporates these factors following IS 10262:2019. The current research aims to create a mix design procedure for high-strength ambient cured GPC by combining the Taguchi method's implementation with the guidelines in IS code. The study also tried to overcome problems of the workability of GPC. A study on the tensile strength of GPC is also incorporated in this work.

## 2 Research Significance

While geopolymer concrete (GPC) offers an effective alternative to traditional cement-based concrete, there is currently no universally accepted standard mix design procedure in place. In the present study, the optimal design mix for geopolymer concrete (GPC) is determined using the Taguchi method taking into account all significant factors that influence workability and strength under ambient curing temperatures. Employing the orthogonal array, Taguchi serves as a dependable design method that effectively reduces unwanted trials. Utilizing the signal-to-noise (S/N) ratio for data examination and forecasting of optimal results, the Taguchi approach proves to be a reliable tool for achieving optimal mix designs. The present study aims to formulate a strength-oriented mix design for GPC, utilizing the Taguchi method.

## 3 Experimental Investigations

### 3.1 Material Study

In the formulation of GPC, the binder materials employed consist of ground granulated blast furnace slag (GGBS)

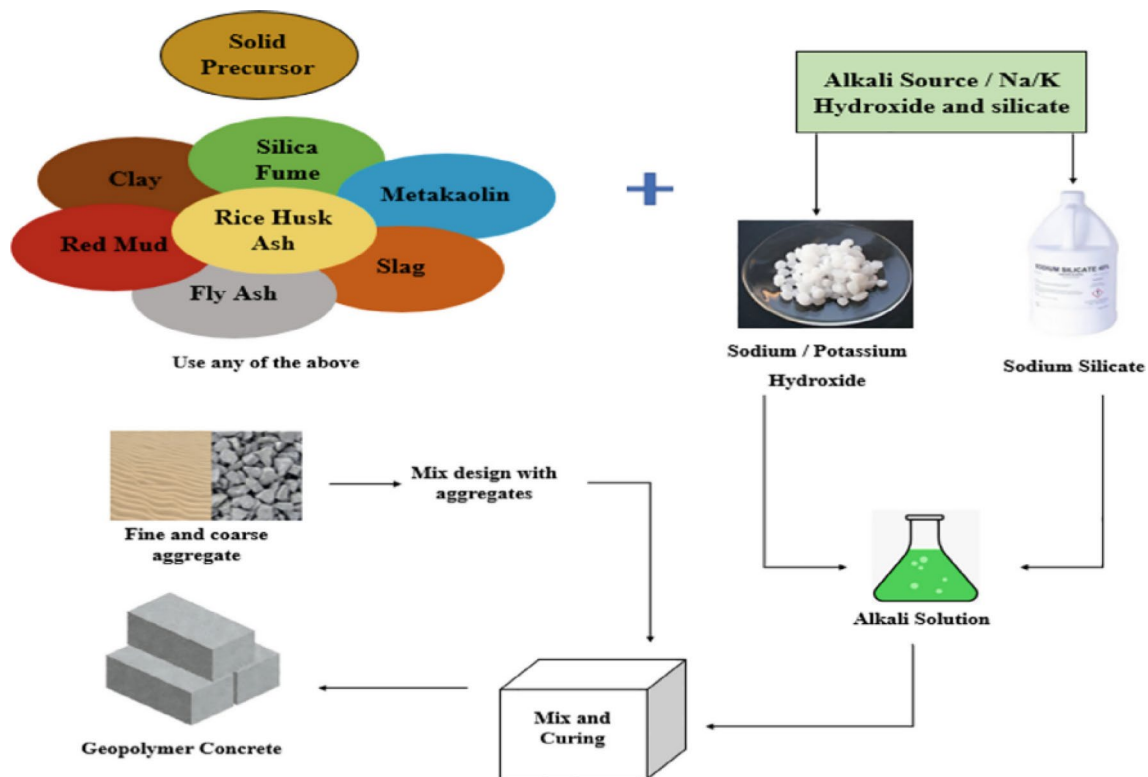


Fig. 1 Production process of geopolymer concrete (Skariah Thomas et al. 2022)

and dolomite. GGBS and dolomite are derived from the steel industry and rock-crushing plants, respectively, as by-products. As per a prior study conducted by Alexander and Shashikala (2022) on GGBS-based geopolymer concrete, the inclusion of GGBS accelerates the polymerization process. This is due to the presence of CaO in GGBS, which not only generates heat but also contributes to the formation of C–S–H gel and N–A–S–H gel. The chemical constituents of GGBS and dolomite are shown in Table 1.

In the research, standard aggregates are utilized in a surface-saturated dry state (SSD) condition. The coarse aggregates were 12.5 mm (specific gravity is 2.47 and water absorption rate 0.66%) and natural sand (Specific gravity 2.53 and water absorption rate is 0.7%) confirming zone 2 as per IS 383:2016 was used as fine aggregates. The particle size distribution curve of aggregates and precursors is shown in Fig. 2. A naphthalene sulphonate superplasticizer, Complast SP430 (IS: 9103:1999) of specific gravity 1.22 supplied by FOSROC, is used for improving the workability of the mix. The activator solution consists of sodium hydroxide in pellet form having a purity 97% dissolved in water and sodium silicate in solution form having SiO<sub>2</sub> (27.2%), Na<sub>2</sub>O (8.9%) and H<sub>2</sub>O (63.9%). For preparing 12 M solutions, 480 g of pellets is dissolved in 1 L of water. These two are mixed to form the activator one day before use.

### 3.2 Mix Design of GPC using L<sup>9</sup> array of Taguchi method

The initial mix design stages are carried out following IS 10262:2019. The input parameters in the IS code-based mix design are the grade of concrete, the size of the aggregate used, the specific gravity of cement and aggregates, workability in terms of the slump, zone of sand, and water absorption of aggregates.

There are no provisions in IS 10262:2019 to accommodate other parameters like binder proportion, the quantity of superplasticizer, ratio of sodium silicate to sodium hydroxide, and molar content. So the Taguchi method is used to incorporate the above-mentioned parameters to arrive at the optimum proportion of GPC (Nazari et al. 2012). The technique employs a unique set of arrays referred to as orthogonal arrays (OA) that examine several variables with a few experiments. When compared to the trial-and-error mix design process, the DOE (design of experiments) employing orthogonal arrays is effective (Türkmen et al. 2008). The OA minimizes variables that are uncontrollable and reduces

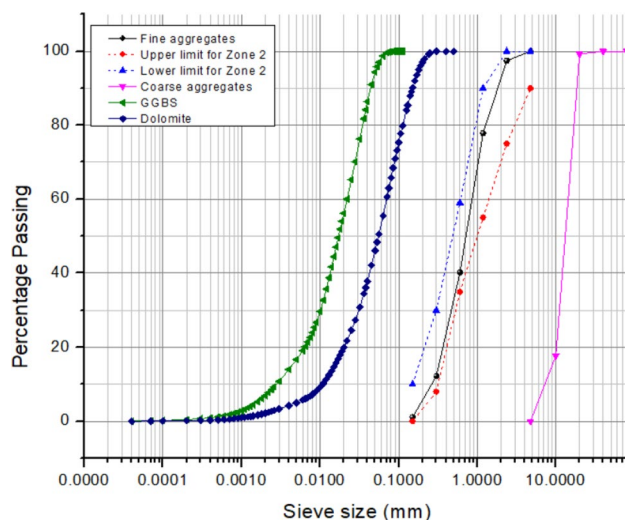


Fig. 2 Sieve analysis of binders and aggregates used in the study

the number of experiments. For instance, the typical factorial design requires 3<sup>4</sup> or 81 test runs when employing four parameters at three proportions, while the Taguchi method employs only 9 test runs. The framework of the study is depicted in Fig. 3.

For optimization, the Taguchi method makes use of the signal-to-noise (S/N) ratio. The S/N ratio supports data analysis and optimal outcome prediction. In short, OA offers a set of tests that are well-balanced, and the S/N ratio acts as an objective function for optimization. The effectiveness, affordability, robustness, and simplicity of output interpretation are the key benefits of the Taguchi method (Hadi et al. 2017). In this work, the L9 orthogonal array in Table 2 is used, which can accommodate 4 factors at three levels.

A distinct combination of binders, the concentration of NaOH in molar form, the ratio of Na<sub>2</sub>SiO<sub>3</sub>/NaOH, and the amount of superplasticizer are all specifically varied in each trial. The ranking of the design parameters is affected by adopting the proper S/N (signal-to-noise ratio). The Taguchi method generally proposes three kinds of S/N ratios: lower, higher, and nominal (Dave and Bhogayata 2020). In the current investigation, the higher the better signal-to-noise ratio was used. The parameters and levels used in the Taguchi mix design are shown in Table 3.

The mixing combinations of GGBS, dolomite, fine aggregates, and coarse aggregates used in the study are shown in Table 4. In addition to the parameters recommended in IS 10262:2019, the present investigation included the

Table 1 Chemical properties of GGBS and dolomite

Oxide	SiO <sub>2</sub> (%)	Al <sub>2</sub> O <sub>3</sub> (%)	Fe <sub>2</sub> O <sub>3</sub> (%)	CaO (%)	MgO (%)	K <sub>2</sub> O (%)	SO <sub>3</sub> (%)	P <sub>2</sub> O <sub>5</sub> (%)
GGBS	35.26	22.94	0.25	25.52	13.26	0.4	1.27	0.038
Dolomite	21.10	6.25	1.62	54.13	16.68	0.56	0.19	0.043

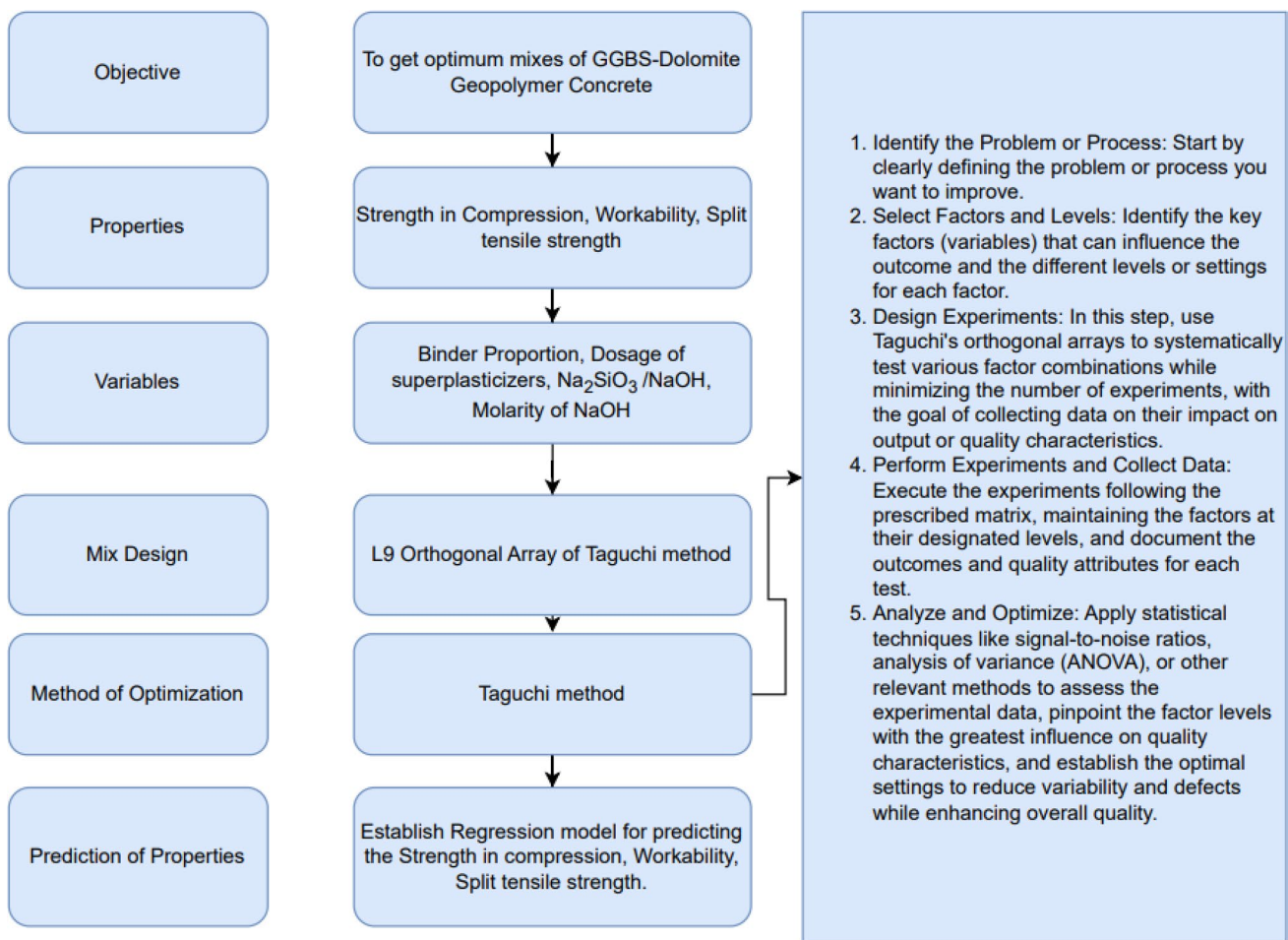


Fig. 3 Framework of the Taguchi design

Table 2 Orthogonal array used in the study

Trial	Variable A	Variable B	Variable C	Variable D
A1	1	1	1	1
A2	1	2	2	2
A3	1	3	3	3
A4	2	1	2	3
A5	2	2	3	1
A6	2	3	1	2
A7	3	1	3	2
A8	3	2	1	3
A9	3	3	2	1

binder proportion, the dosage of superplasticizer, the  $\text{Na}_2\text{SiO}_3$ -to- $\text{NaOH}$  ratio, and the molarity of  $\text{NaOH}$ . The levels of each factor were taken based on the previous studies (Saranya et al. 2020); (Saranya et al. 2021); (Saranya et al. 2019b) and some trials. The reasonable limits are numbered from 1 to 3, with 3 being the highest.

Table 3 Parameters and levels used in the mix design

Variable	Level 1	Level 2	Level 3
A Binder proportion	B1*	B2*	B3*
B Superplasticizer dosage	1.25	1.5	1.75
C $\text{Na}_2\text{SiO}_3/\text{NaOH}$ Ratio	1.5	2	2.5
D Molarity of $\text{NaOH}$	12	13	14

B1 = 70% GGBS 30% dolomite, B2 = 80% GGBS 20% dolomite, B3 = 90% GGBS 10% dolomite

The condition of curing whether ambient or high temperature and strength attainment of geopolymer concrete depends upon the type of alumino-silicate base materials used in the mix (Fernández-Jiménez et al. 2005). So the combination of alumino-silicate precursors such as GGBS and dolomite are taken as variable A. Based on the trials, the mix resulting from GGBS and dolomite is found to be less workable without the usage of a superplasticizer. So to improve the workability of the mix, the dosage of

**Table 4** Mixing combinations of GGBS, dolomite, fine aggregates, coarse aggregates, superplasticizer

Exp no.	A	B	C	D	GGBS (kg/m <sup>3</sup> )	Dolomite (kg/m <sup>3</sup> )	F.A (kg/m <sup>3</sup> )	C.A (kg/m <sup>3</sup> )	Na <sub>2</sub> SiO <sub>3</sub> (kg/m <sup>3</sup> )	NaOH (kg/m <sup>3</sup> )	S.P (kg/m <sup>3</sup> )
1	B1	1.25	1.5	12	298.71	128.02	757.36	976	128.02	85.35	5.33
2	B1	1.5	2	13	298.71	128.02	757.36	976	142.25	71.12	6.40
3	B1	1.75	2.5	14	298.71	128.02	757.36	976	152.41	60.96	7.46
4	B2	1.25	2	14	341.40	85.35	757.36	976	142.25	71.12	5.33
5	B2	1.5	2.5	12	341.40	85.35	757.36	976	152.41	60.96	6.40
6	B2	1.75	1.5	13	341.40	85.35	757.36	976	128.02	85.35	7.46
7	B3	1.25	2.5	13	384.06	42.67	757.36	976	152.41	60.96	5.33
8	B3	1.5	1.5	14	384.06	42.67	757.36	976	128.02	85.35	6.40
9	B3	1.75	2	12	384.06	42.67	757.36	976	142.25	71.12	7.46

superplasticizer is taken as variable B. Further, the reaction between aluminosilicate precursors and activators like NaOH and Na<sub>2</sub>SiO<sub>3</sub> depends on the oxide concentration and molarity of NaOH and Na<sub>2</sub>SiO<sub>3</sub>/NaOH (Lee et al. 2014). Additionally, the creation of a more densely packed polymeric structure with greater strength requires an optimal amount of silica content. However, too much sodium silicate slows the polymerization process by preventing water evaporation (Alexander and Shashikala 2022). So the SS/SH ratio and molarity of NaOH are taken as variables C and D, respectively.

Variable A represents different proportions of aluminosilicate precursors GGBS and dolomite. The maximum adopted dolomite proportion is 30%. Low compressive strength may result from more than 30% of dolomite (Saranya et al. 2019a). Variable B indicates the dosage of superplasticizer. The development of M45 grade GPC is the main goal of the present investigation. A superplasticizer based on naphthalene was used to retain the mix's viscosity and to decrease the amount of water that was needed (Rattanasak and Chindaprasirt 2009). The minimum superplasticizer dosage was taken as 1.25% of the total binder content at level 1 and 1.75% of the binder content at the third level. The inclusion of silicate aids in the polymerization process. But overdosage of the same will retard the process (Ferdous et al. 2013). So the ratio Na<sub>2</sub>SiO<sub>3</sub>/NaOH is taken as variable C. The ratio is 1.5 at first level and 2.5 at third level. Variable D is the molarity. Its value is 12 M at level 1 and 14 M at level 3. A minimum 10 M solution is necessary for efficient polymerization (Nath and Sarker 2014). The compressive strength is usually proportional to the molar content of NaOH. But higher molar content is not recommended for GPC because of the formation of improper structures due to the faster polymerization (Deb et al. 2015). So, in this study, molar concentration is limited to 14 M (Cao et al. 2018).

### 3.3 Testing of Specimen

According to 516: 1959, cylinders of 150 mm diameter and 300 mm height are used for split tensile strength tests, whereas 100-mm cubes are used for compressive strength tests. The GPC mix has a more cohesive nature than ordinary concrete during specimen vibration due to the effect of GGBS (Dave and Bhogayata 2020); (Skariah Thomas et al. 2022). The mixing, placement, and compaction are completed within 30 min. The workability tests on fresh mixes are done before casting. The slump test was conducted according to ASTM C 143. Ambient curing at 32 °C for 24 h is adopted. All specimens undergo strength tests after the 7-day curing period. Three cubes and three cylinders are subjected to compressive strength testing and split tensile strength testing for each mix. All the mixes developed in the work have sufficient workability. Figure 4c shows the specimens cast and the specimens subjected to ambient curing. The test setup for compressive strength and split tensile strength is depicted in Fig. 4d and e.

## 4 Results and Discussion

### 4.1 Workability

The liquid content in the fresh mix, the binder type, and the superplasticizer dosage all affect the workability of the fresh mix. A slump value of 150 mm was adopted for all the mixes in the work and liquid content is modified according to the provisions from IS 10262:2019. The test was conducted immediately after the mix is prepared.

The addition of dolomite to GPC enhanced the workability, according to the slump tests. It was noticed that the new GPC exhibited good workability with suitable slump values (Fig. 5). Figure 4b shows the slump test on GPC. All of the mixes had a similar response. It is found that the



Fig. 4 a GPC mix in pan mixer b slump test c Cast specimens subjected to ambient curing e Split tensile strength test f Compressive strength test

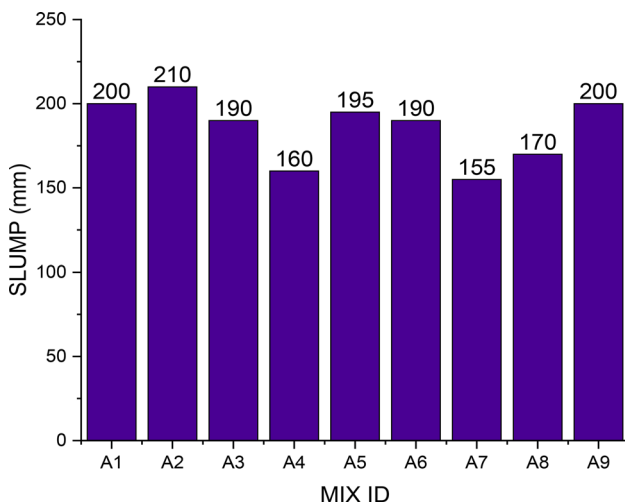


Fig. 5 Slump values for GGBS–dolomite GPC

rheological characteristics of GPC are similar to how ordinary concrete responds. Figure 4a represents fresh GPC mix in a pan mixer.

#### 4.1.1 Taguchi Optimization

The OA (orthogonal array) used in this work requires only 9 test runs. It uses a signal/noise (S/N) ratio to cut down on meaningless trials and aid in input parameter optimization. This aids in data interpretation and the forecasting of optimized results. In this context, the term ‘signal’ refers to the desirable value or the response variable, while ‘noise’ represents the undesirable value or the standard deviation. The signal-to-noise (S/N) ratio serves as a metric to quantify the level of variation present in the response variable. The objective is to optimize and maximize this S/N ratio, thereby enhancing the quality of the signal while minimizing the impact of undesirable variations or noise. The

signal-to-noise ratio (S/N) can be broadly categorized into three main equations, denoted as (1), (2), and (3) as follows:

$$\frac{S}{N} = -10 \times \log_{10} \left( \frac{1}{n} \sum_{i=1}^n (Y_i - Y_0)^2 \right) \quad (1)$$

$$\frac{S}{N} = -10 \times \log_{10} \left( \frac{1}{n} \sum_{i=1}^n (Y_i)^2 \right) \quad (2)$$

$$\frac{S}{N} = -10 \times \log_{10} \left( \frac{1}{n} \sum_{i=1}^n (1/Y_i)^2 \right) \quad (3)$$

S/N represents the signal-to-noise ratio, ‘n’ stands for the number of experiments conducted, ‘ $Y_i$ ’ denotes the response variable targeted for optimization, and ‘ $Y_0$ ’ represents the mean of the responses. Equation (1) illustrates a value indicating that the nominal combination is most suitable for optimization (nominal is better). In contrast, Eq. (2) is employed when seeking the optimal mix where smaller parameters are better fitted (smaller is better). Equation (3) highlights the largest values as being the most fitting in the context of optimization (larger is better).

In the context of strength and workability, the preference is for obtaining the maximum or largest value. Therefore, Eq. (3) is applied specifically for assessing and optimizing strength and workability.

In reality, the OA offers a group of well-organized trials, and the ratio S/N acts as an effective optimization tool (Dave and Bhogayata 2020). The result analysis is done using the software Minitab 2020 and is represented in Figs. 6 and 7. For each level of all mix design parameters, the Minitab

calculates a unique S/N ratio. The GPC’s characteristics and type of test guide the choice of various S/N ratios.

#### 4.1.2 Workability Result Analysis

The workability should be high for better handling of fresh concrete. So, the S/N ratio criteria used here are larger and better. Unlike earlier research, which solely examined the effect of binder proportion on workability (Saranya et al. 2019a), the current study demonstrates the dependence of each parameter on workability. As shown in Fig. 6, B1 exhibits the highest mean value of 200 mm among the three variations in binder content, whereas 1.75% dosage of superplasticizer exhibits the highest mean slump value of 193.3 mm. Also, the optimum value of 190 mm is obtained at a molar content of 12.

For each specific response characteristic, such as the S/N ratio, standard deviation and mean value, Minitab generates a response table. The variable that has a major influence on the result is highlighted in the response table, along with the level of the factor that produces a lower or higher response characteristic value.

Figure 7 presents contour plots that illustrate how various mix design variables affect workability. The highest workability was obtained for proportion B1 which contains the maximum amount of dolomite of all the worked-out mixes. The addition of dolomite to GPC improves workability due to its large surface area. The additional water added to the prepared mix makes up 15% of the binder content. The highest slump can be obtained by choosing a specific range of factors. For example, a slump value of more than 200 mm is achieved for proportion B1, with dosages of SP between 1.3 and 1.6% of binder content, the

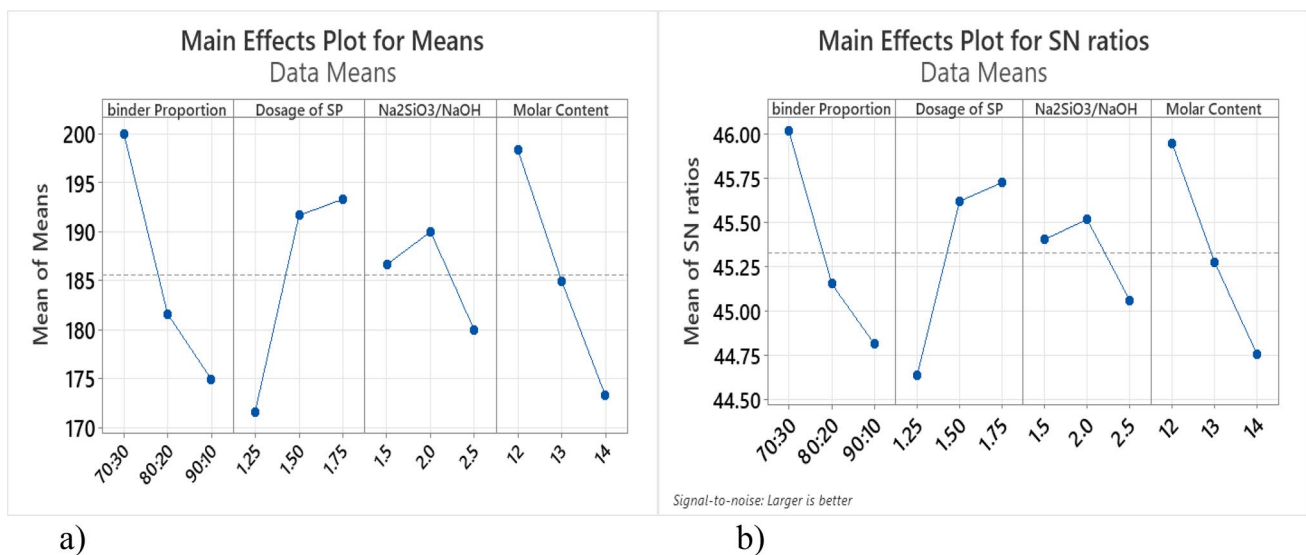
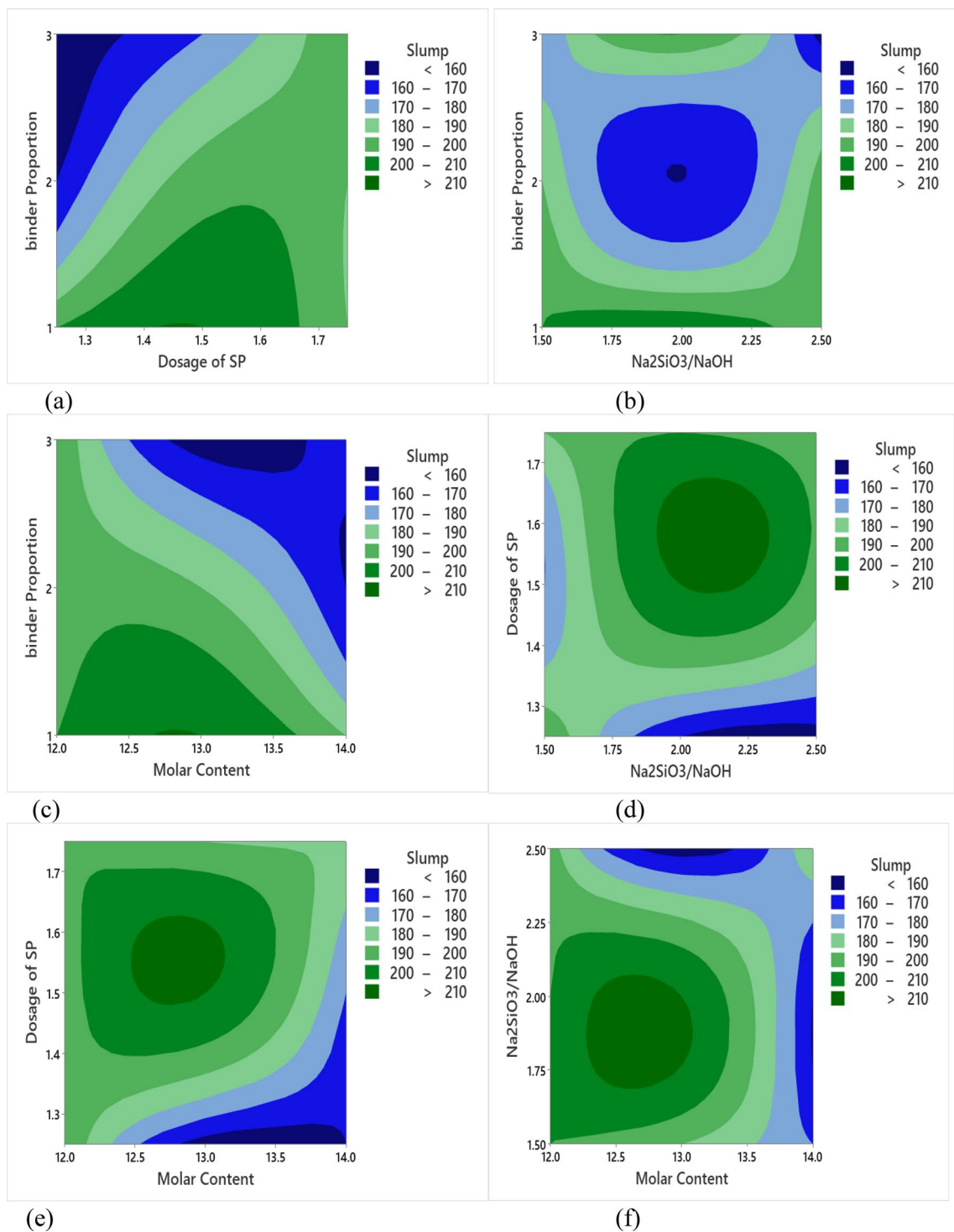


Fig. 6 a Optimized levels of means for slump, b optimized levels of S/N ratios for slump (Criteria: Larger is better for workability)





**Fig. 7** a–f Bivariate relationship between variables and slump

ratio  $\text{Na}_2\text{SiO}_3/\text{NaOH}$  of 1.5–2.25 and molarity of NaOH varies from 12 to 13.5 (Fig. 7a, b, c). Similarly, the dosage of SP varied from 1.5 to 1.6% of binder content, the ratio  $\text{Na}_2\text{SiO}_3/\text{NaOH}$  of 1.75–2.25, and the molarity range of

12.5–13 M will all result in slump values more than 200 for any proportions used (Fig. 7d, e, f).

The binder content was the factor that had the highest influence on the design mix (Tables 5 and 6) followed by

**Table 5** Results of the means and the ranking of parameters from the MINITAB for workability

Level	Binder proportion	Dosage of plasticizer	Na <sub>2</sub> SiO <sub>3</sub> /NaOH	Molar value
1	200.0	171.7	186.7	198.3
2	181.7	191.7	190	185
3	175	193.3	180	173.3
Delta	25	21.7	10	25
Rank	1	3	4	2

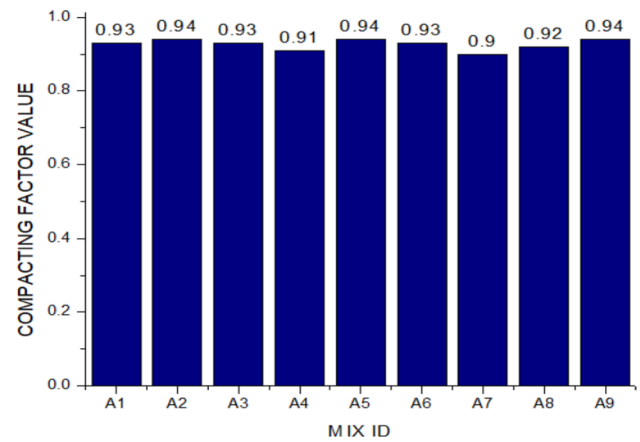
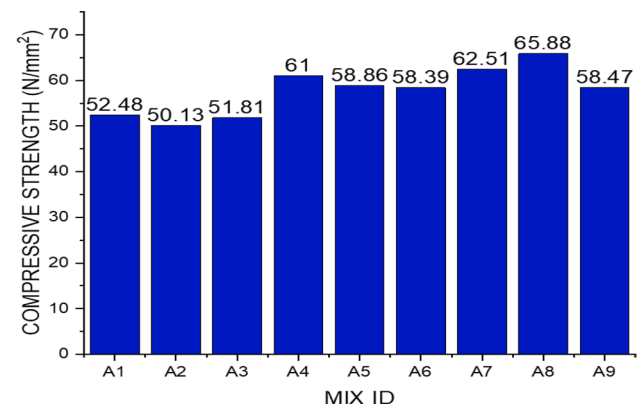
**Table 6** Results of the S/N ratio and the ranking of parameters from the MINITAB for Workability

Level	Binder proportion	Dosage of plasticizer	Na <sub>2</sub> SiO <sub>3</sub> /NaOH	Molar value
1	46.01	44.64	45.40	45.95
2	45.15	45.62	45.52	45.28
3	44.81	45.72	45.06	44.76
Delta	1.20	1.09	0.45	1.19
Rank	1	3	4	2

the molarity of NaOH, and dosage of the superplasticizer. Additionally, the B3 level provided the lowest mean value for the S/N ratio because B3 has a higher proportion of slag (90% GGBS) significantly reducing the workability of GPC. B1, on the other hand, exhibited an increase in workability due to its lower percentage of GGBS (70% GGBS) (Dave and Bhogayata 2020); (Skariah Thomas et al. 2022). The optimum value of the mean S/N ratio was displayed by the superplasticizer, which made up 1.75% of the binder content. Figure 6 indicates that the optimum Na<sub>2</sub>SiO<sub>3</sub>/NaOH ratio was 2. For improved workability, the 12 M solutions are found to be helpful.

#### 4.1.3 Compaction Factor Test

In addition to slump test, compaction factor test is also done for 9 mixes and the results are shown in Fig. 5. While the slump test offers information about the consistency of the concrete, the compaction factor test assesses the ability of the mix to self-compact and fill voids effectively. Compaction factor test is done according to IS 1199 (Part 2): 2018. Based on the data presented in Fig. 8, it is evident that the compaction factor values for all the mixes exceed 0.9, signifying a significantly high level of compactability for each mix.

**Fig. 8** Compaction factor values for GGBS–dolomite GPC**Fig. 9** Compressive strength test results of nine trial mixes**Table 7** Results of the means and the ranking of parameters from the MINITAB for strength in compression

Level	Binder proportion	Dosage of plasticizer	Na <sub>2</sub> SiO <sub>3</sub> /NaOH	Molar value
1	51.47	58.66	58.92	56.60
2	59.41	58.29	56.53	57.01
3	62.29	56.22	57.72	59.56
Delta	10.81	2.44	2.38	2.96
Rank	1	3	4	2

## 4.2 Mechanical Properties

### 4.2.1 Strength in Compression

Compressive and split tensile strength tests were done to examine the mix design developed using the L9 OA of the Taguchi method. Seven days of ambient curing is adopted for all the specimens. Figure 9 depicts the result of the

**Table 8** Results of the S/N ratio and the ranking of parameters from the MINITAB for strength in compression

Level	Binder proportion	Dosage of plasticizer	Na <sub>2</sub> SiO <sub>3</sub> /NaOH	Molar value
1	34.23	35.34	35.37	35.05
2	35.48	35.26	35.02	35.08
3	35.88	34.98	35.20	35.46
Delta	1.65	0.36	0.35	0.41
Rank	1	3	4	2

compressive strength test of nine mixes. Each of the nine results is equal to the mean of the results of three specimens. According to Fig. 9, trial mix 8 had the greatest value, 65.88 MPa, while trial mix no 2 had the lowest value, 50.13 MPa.

Tables 7 and 8 indicate that the higher the percentage of GGBS content, the higher the strength. This might be because more dissolved calcium from the surface of the GGBS is causing a higher rate of C–S–H gel formation (Salih et al. 2015). Molar content is the second-most significant factor. With the increase in the molar content of NaOH, the compressive strength of the geopolymers also increases. This is because higher NaOH concentrations were more effective at dissolving the source particles, which improved the polymerization and thus strength (Mathew and Issac 2020); (Unis Ahmed et al. 2022); (Sudhakumar).

From Tables 6 and 7, it is clear that the strength in compression of GGBS–dolomite GPC is least affected by Na<sub>2</sub>SiO<sub>3</sub>/NaOH value. According to the current study, to obtain good results in compressive strength, a dosage of 1.25% superplasticizer with a Na<sub>2</sub>SiO<sub>3</sub>/NaOH value of 1.5 is to be used. The dosage of superplasticizer above this level decreases the strength of GPC maybe due to the formation of a thin layer on the source particles preventing the polymerization and resulting in a few unreacted particles (Dave and Bhogayata 2020).

Figure 10 represents contour plots showing the relationship between mix design variables and the compressive strength of the specimen. Figure 11 shows the main effects plot for means and S/N ratio of compressive strength.

From Fig. 10a, it is clear that for the dosage of superplasticizer varying from 1.3 to 1.5% and binder proportion, B3 gives higher compressive strength. In all the cases, binder proportion B3 gives higher compressive strength. Similarly, for binder proportion B3, Na<sub>2</sub>SiO<sub>3</sub>/NaOH value of 1.5 and molarity of 14 M give higher compressive strength (Fig. 10b and c). For any binder proportion, the dosages of SP range from 1.3 to 1.6, the molar value of 14 and Na<sub>2</sub>SiO<sub>3</sub>/NaOH of 1.5 gives a better compressive strength always (Fig. 10d, e, f). In this case, compressive strength obtained for all the

mixes are above 45 MPa so the IS code procedure can effectively be used for the GPC mix design.

#### 4.2.2 Split Tensile Strength

Figure 12 depicts the split tensile strengths obtained from the L9 orthogonal array provided by the Taguchi approach. The maximum strength is obtained for A8 with binder proportion B3, the dosage of superplasticizer of 1.5%, 14 M NaOH solution and Na<sub>2</sub>SiO<sub>3</sub>/NaOH ratio of 1.5. The highest split tensile strength is obtained for binder proportion B3 similar to the compressive strength test. This may be due to a greater rate of C–S–H, N–S–H and N–A–S–H gel formation brought on by more dissolved calcium from the GGBS surface (Salih et al. 2015). The minimum strength is obtained for specimen T1 with a B1 binder proportion, the dosage of superplasticizer of 1.25%, 12 M NaOH solution and Na<sub>2</sub>SiO<sub>3</sub>/NaOH ratio of 1.5 due to a lower percentage of GGBS and lower molar value.

Tables 9 and 10 present the outputs of the Taguchi analysis. The outcomes once more revealed how crucial binder proportion is. The delta value of the means indicates that the molarity of NaOH and the ratio of Na<sub>2</sub>SiO<sub>3</sub>/NaOH have an equal effect on tensile strength. Figure 10 shows the contour plots showing the relationship between the split tensile strength and various mix design parameters. It is clear that from Fig. 13, for binder proportion B3, molarity range of 13–14 M, Na<sub>2</sub>SiO<sub>3</sub>/NaOH range of 1.5–2.0, and superplasticizer dosage range of 1.4–1.7 give split tensile strength greater than 3.6 MPa (Fig. 13(a, b, c)). Figure 14 depicts the response of the Taguchi analysis. From Fig. 14, it is understood that the binder proportion B3, the superplasticizer dosage of 1.5%, Na<sub>2</sub>SiO<sub>3</sub>/NaOH ratio of 2, and molarity of 14 M give the maximum value due to maximum GGBS content and higher molarity.

The optimal combination of the mix design parameters for improving compressive and tensile strength as well as workability are shown in Table 11. These are the outcomes of the analysis. The Taguchi method and the recommendations from IS 10262:2019 were combined to develop the mix design. All the fresh and hardened properties were evaluated based on the higher S/N criteria.

The current study demonstrated the efficiency of the adopted approach for optimizing the constituents of the GPC to achieve the desired strength of the mix by investigating the compressive and splitting tensile strength.

The error resulting from compressive strength test and split tensile strength tests is depicted in Table 12. From Table 12, mixes 1, 3, and 6 showed less standard deviation, indicating that the test results were less variable and consistent. On the contrary, mixes 7 and 8 showed higher standard

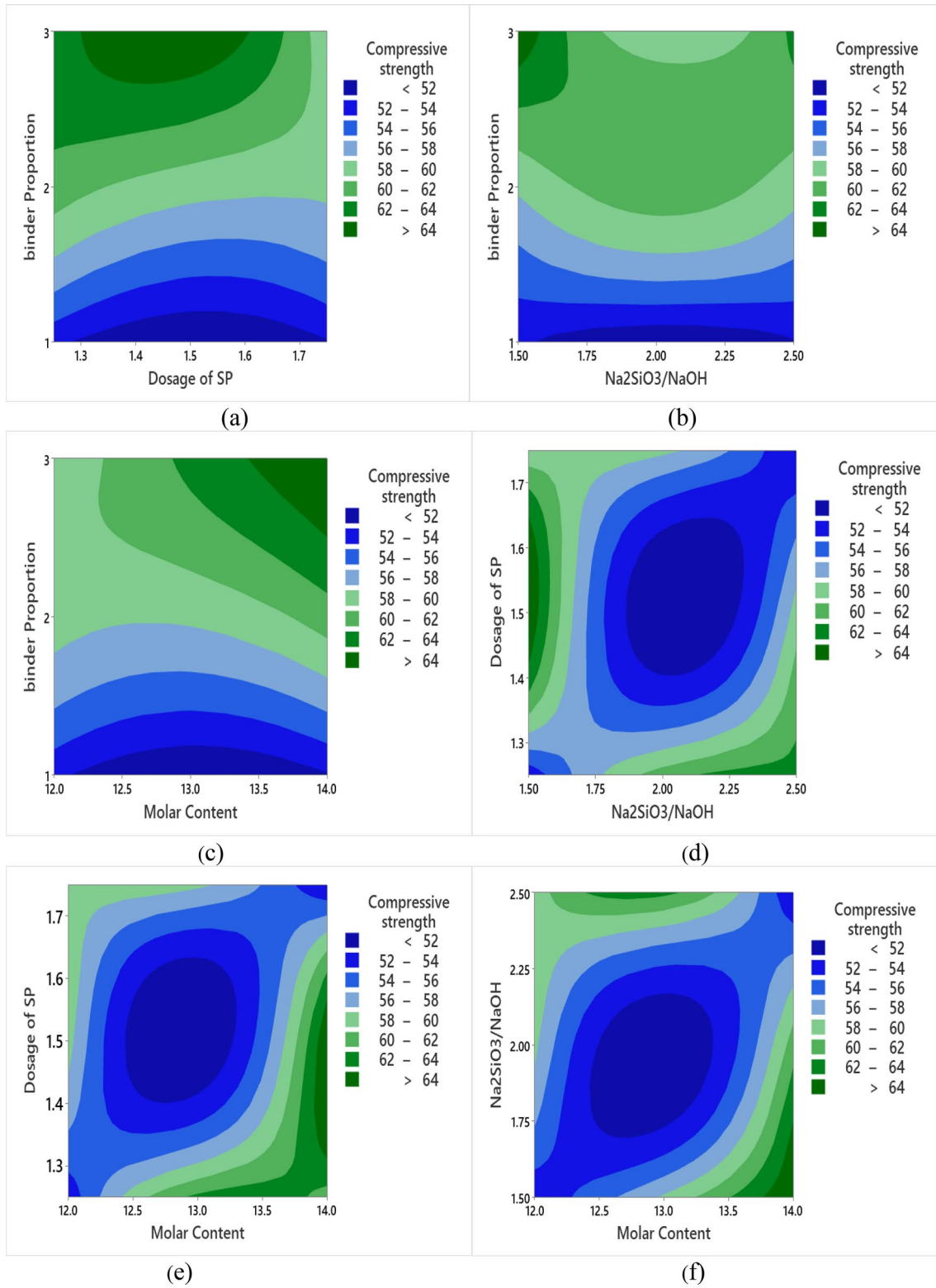


**Fig. 10** a–f Bivariate relationship between variables and compressive strength

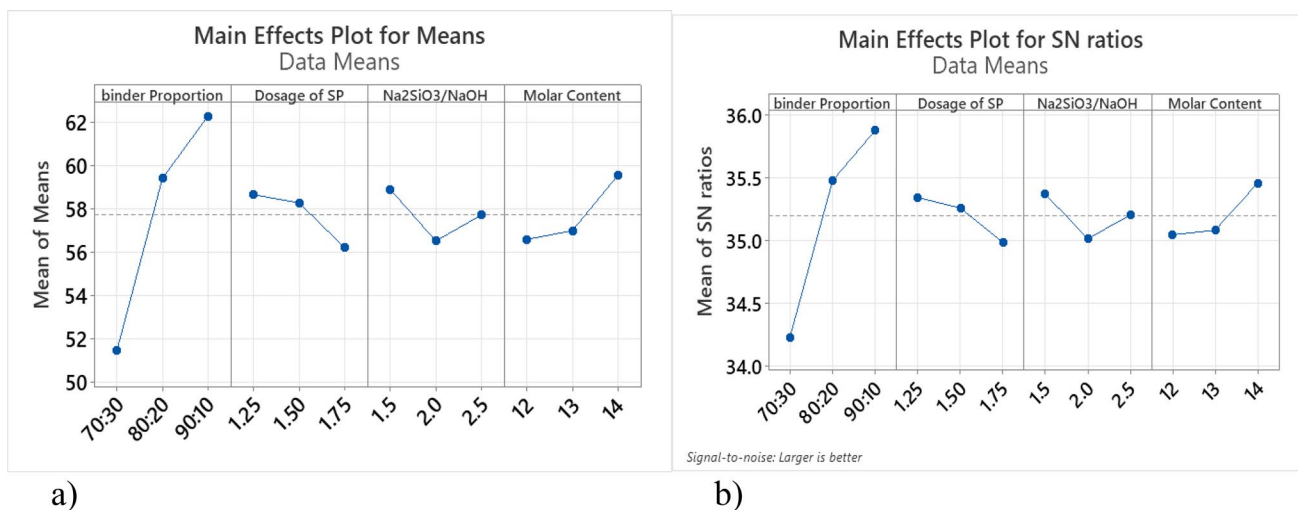


**Fig. 11** a Optimized levels of means for compressive strength and b optimized levels of S/N ratios for compressive strength (Criteria: Larger is better for Compressive strength)

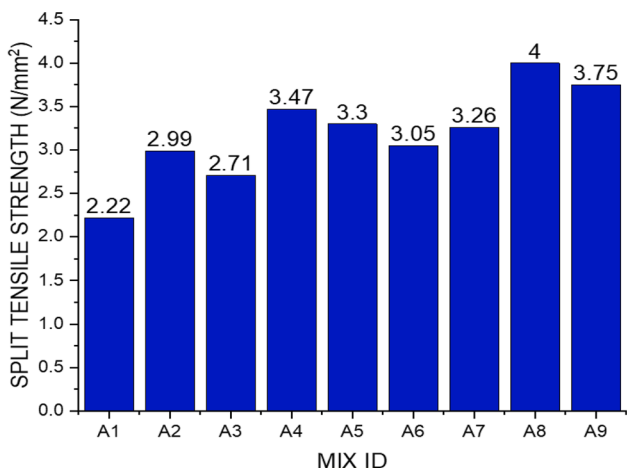


**Fig. 12** Split tensile strength of the trial mix

**Table 9** Results of the means and the ranking of parameters from the MINITAB for split tensile strength

Level	Binder proportion	Dosage of plasticizer	Na <sub>2</sub> SiO <sub>3</sub> /NaOH	Molar value
1	2.639	2.985	3.092	3.092
2	3.277	3.430	3.402	3.101
3	3.670	3.171	3.092	3.393
Delta	1.032	0.444	0.310	0.301
Rank	1	2	3	4

deviations, indicating greater variability in strength. This could have been attributed to the variability of the mixing process.

**Table 10** Results of the S/N ratio and the ranking of parameters from the MINITAB for Split tensile strength

Level	Binder Proportion	Dosage of Plasticizer	Na <sub>2</sub> SiO <sub>3</sub> /NaOH	Molar value
1	8.363	9.339	9.557	9.598
2	10.297	10.641	10.596	9.824
3	11.263	9.945	9.770	10.502
Delta	2.900	1.302	1.039	0.904
Rank	1	2	3	4

### 5 Analysis of Variance (ANOVA)

The influence of individual factors on compression strength, workability, and split tensile strength was evaluated using an analysis of variance, with a 95% confidence interval, to determine their respective contributions. Based on Fig. 15, it is evident that the binder proportion exerts the most significant influence on both compression strength and split tensile strength, accounting for 89.13 and 91.76% of the variation, respectively. Following this, the molarity of NaOH demonstrates a comparable contribution of 5.9% to each of these strength characteristics. Enhancing the binder content and molarity results in higher strength in compression and split tensile strength, as a greater quantity of CaO from GGBS undergoes dissolution, leading to the formation of polymerization products (Mathew and Issac 2020). Additionally, there are studies indicating that the concentration of NaOH facilitates both the dissolution process and the bonding of solid particles within the geopolymeric environment (Guo et al. 2010).

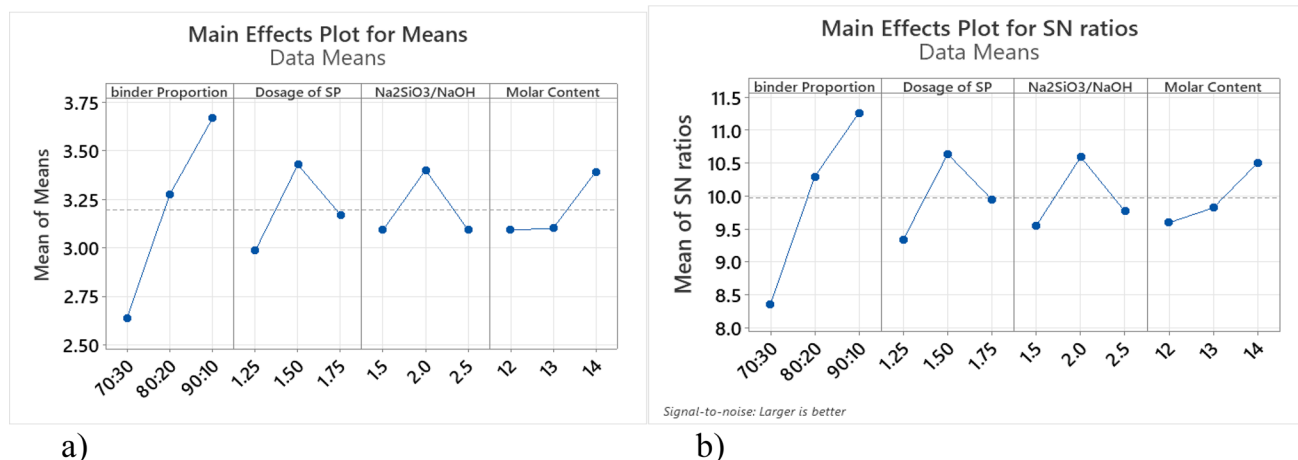


**Fig. 13** a Optimized levels of means for split tensile strength and b optimized levels of S/N ratios for split tensile strength (Criteria: Larger is better for Split tensile strength)

On the contrary, the Na<sub>2</sub>SiO<sub>3</sub>/NaOH ratio and superplasticizer dosage exhibited minor contributions, each accounting for less than 5%. This observation is supported by the strength outcomes, as concrete with high strength levels exceeding 50 MPa can be produced irrespective of variations in the Na<sub>2</sub>SiO<sub>3</sub>/NaOH ratio and superplasticizer dosage. These findings indicate the dominant influence of binder proportion and NaOH molarity in governing the mechanical and durability properties of GGBS–dolomite GPC.

Moreover, the influence of binder proportion and molarity on workability demonstrated significant magnitudes, leading to 42.52 and 31.54%, respectively. Likewise, the Na<sub>2</sub>SiO<sub>3</sub>/NaOH ratio and superplasticizer dosage contributed 23.69 and 2.24%, respectively. In contrast to their influence on strength characteristics, these factors exert a notable effect on workability, highlighting their non-negligible role. However, achieving satisfactory workability of GPC for various applications is still possible.

## 6 Regression Equations and Prediction of the Responses

Regression analysis serves as a statistical tool used to explore and examine relationships among variables. The correlation coefficient, denoted as R-Sq, should ideally fall within the range of 80 to 100% in multiple linear regression analyses. The R-Sq value serves the purpose of predicting future outcomes based on related data. It quantifies the extent to which the model can accurately predict results, indicating the model's predictive reliability. A linear model was formulated to establish a relationship between the mix properties and the parameters employed.

The regression equations developed and R<sup>2</sup> values are shown in Table 13.

As indicated earlier, the Taguchi method used orthogonal arrays to minimize the number of trials, optimization, and prediction. As a result, numerous combinations of factor levels have been omitted from the designed experiments, but these still require prediction. Out of a total of 81 possible combinations (calculated as 3<sup>4</sup>), only 9 experiments were designed and subsequently tested. Hence, predictions using the regression equations were created to estimate the outcomes associated with various factor combinations for slump, compressive strength, and split tensile strength. Figure 16 displays the linear fit of the predicted vs. experimental results and the prediction error.

For evaluating the prediction performance accurately, the mean absolute percentage error (MAPE) value corresponding to each property prediction is displayed in Fig. 16b, d and f, respectively. It is calculated by the following equation.

$$\text{MAPE} = \frac{100}{N} \sum_j \frac{y_j - x_j}{y_j} \quad (4)$$

where  $y_j$ ,  $x_j$  and  $N$  are the experimental value, predicted value, and number of data, respectively. From Fig. 16, it becomes evident that the correlation coefficient of slump and workability is high (R<sup>2</sup>=0.89 for each) resulting in a lower average prediction error of 2.59 and 2.21, respectively (MAPE). However, when it comes to split tensile strength, the correlation coefficient (R-Sq) is notably lower (R<sup>2</sup>=0.77), leading to a higher MAPE value of 7.381.

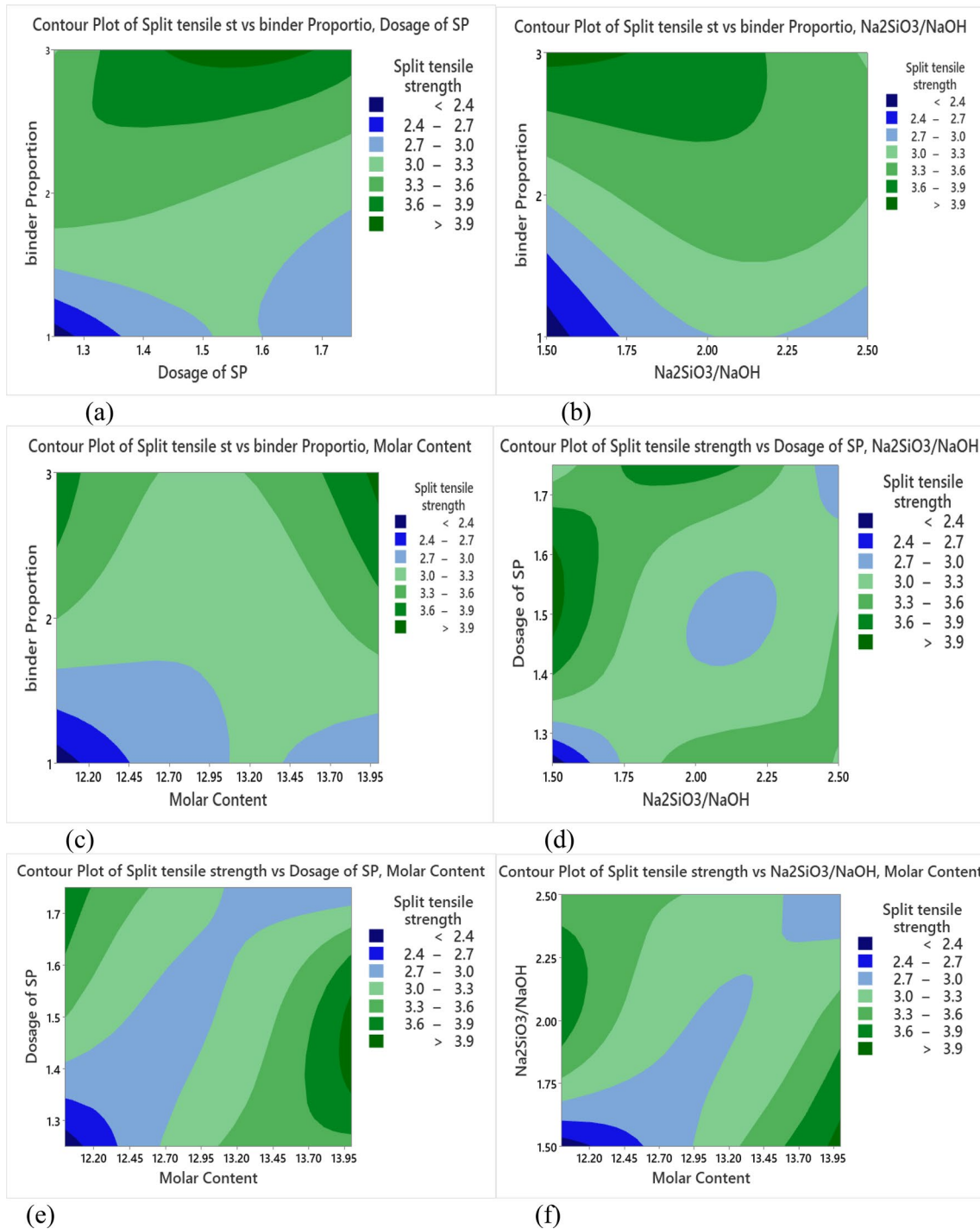


Fig. 14 a–f Bivariate relationship between variables and split tensile strength

### 7 Microstructural Characteristics

From the ANOVA results, the most influencing factor that effects the strength characteristics is the binder proportion.

So, SEM (scanning electron microscopy), EDX (energy-dispersive X-ray spectroscopy) analysis are performed on the 3 samples which is having B1(G70:D30), B2(G80:D20), and B3(G90:D10) proportions.

**Table 11** Error resulting from compressive strength test and split tensile strength tests

Mix ID	Compressive strength (MPa)	± Standard deviation (MPa)	95% confidence interval	Split tensile strength (MPa)	± Standard deviation (MPa)	95% Confidence interval
1	52.48	± 2.50	[50.98, 54.98]	2.22	± 0.30	[1.92, 2.52]
2	50.13	± 2.80	[47.33, 52.93]	2.99	± 0.40	[2.59, 3.39]
3	51.81	± 2.60	[49.21, 54.41]	2.71	± 0.35	[2.36, 3.06]
4	61	± 3.10	[57.90, 64.10]	3.47	± 0.45	[3.02, 3.92]
5	58.86	± 2.90	[55.96, 61.76]	3.3	± 0.38	[2.92, 3.68]
6	58.39	± 2.70	[55.69, 61.09]	3.05	± 0.32	[2.73, 3.37]
7	62.51	± 3.00	[59.51, 65.51]	3.26	± 0.42	[2.84, 3.68]
8	65.88	± 3.40	[62.48, 69.28]	4	± 0.55	[3.45, 4.55]
9	58.47	± 2.75	[55.72, 61.22]	3.75	± 0.48	[3.27, 4.23]

**Table 12** Optimum levels of mix design variables of considered properties

Properties	Optimum levels of mix design variables				Optimization criteria
	Binder proportion	Dosage of super-plasticizer (%)	Na <sub>2</sub> SiO <sub>3</sub> /NaOH	Molarity of NaOH	
Workability	B1	1.75	2	12 M	Larger is better
Compressive strength	B3	1.25	1.5	14 M	Larger is better
Split tensile strength	B3	1.5	2	14 M	Larger is better

## 7.1 SEM with EDX Analysis

The SEM with EDX analysis of geopolymer concrete samples are shown in Fig. 17(a, b and c). In these figures, the microstructural images of the samples B1(G70:D30), B2(G80:D20), and B3(G90:D10) at the age of 28 days is depicted. The microstructure of G70:D30 shown in Fig. 17a reveals the presence of voids as well as numerous microcracks. This clearly contributed to the significantly low strength observed in Sect. 4.2.1. When compared to Fig. 17a, Fig. 17e depicts a greater amorphous character, signifying a higher degree of compactness in G90:D10, with no observable cracks. From EDX analysis, all the mixes taken for study contains higher amounts of silica, aluminium, sodium and calcium, which indicates the presence of NASH (sodium alumino-sulphate) and CASH (calcium alumino-silicate hydrate). When the content of calcium compounds is elevated in geopolymer concrete by adding more ground granulated blast furnace slag, the resulting reaction produces calcium alumino-silicate hydrate (CASH) as a prominent product (Salih et al. 2015). So, CASH is the predominant geopolymer gel which is formed in this scenario. The percentage of elements by EDX analysis is shown in Table 14. From Table 14, the value of Si/Al is above 2.5 for all mixes which indicate formation of 3D networked polysialate-siloxo and polysialate-disiloxo polymers (Silva et al. 2007).

## 8 CO<sub>2</sub>-Assessment of GGBS–dolomite GPC

According to the research conducted by Yang et al. (2013), the calculation of CO<sub>2</sub> emissions is divided into four distinct phases: the material phase (CO<sub>2-M</sub>), transportation phase (CO<sub>2-T</sub>), production phase (CO<sub>2-P</sub>), and curing phase (CO<sub>2-C</sub>). Material phase consists of binders like GGBS, dolomite, alkali activator, fine aggregate, and coarse aggregate. The transportation stage consists of the movement of materials to the concrete plant as well as the transportation of precast materials to the construction site. The production phase involves the CO<sub>2</sub> emissions generated during the operation of a concrete mixer. The curing phase encompasses CO<sub>2</sub> emissions arising from the curing process, including emissions associated with activities such as steam curing. The total CO<sub>2</sub> emission is calculated based on Eq. (5) (Yang et al. 2013).

$$\text{Total CO}_2 = \text{CO}_{2-M} + \text{CO}_{2-T} + \text{CO}_{2-P} + \text{CO}_{2-C} \quad (5)$$

CO<sub>2</sub> emissions for various materials are established using data sourced from the Korean LCI database. In instances where LCI data are unavailable, reference is made to the JSCE (Japanese database). The transportation of binders is assumed to be carried out via bulk trailers, while fine and coarse aggregates are transported using drum trucks with a 15-ton capacity. Also, CO<sub>2-M</sub> and CO<sub>2-T</sub> can be found by Eqs. (6) and (7), respectively.



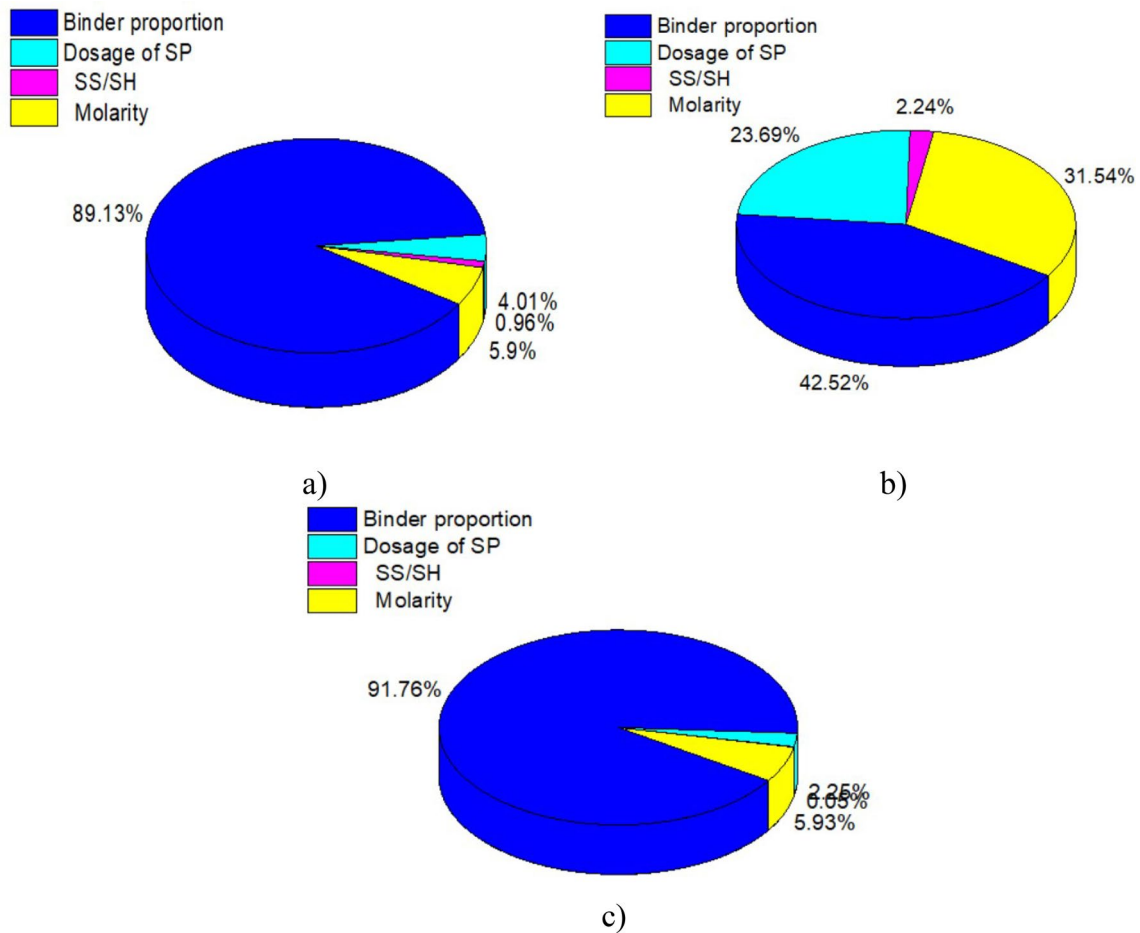


Fig. 15 Contribution of each factor towards a strength in compression, b workability, c split tensile strength

Table 13 Regression equations for slump, compressive strength, and split tensile strength

Models	Model summary
Slump = 321.4 - 12.50A + 43.3B - 6 - 67C - 12.50D	R-Sq = 89.02% R-Sq(adj) = 78.04% S = 9.03312
Strength in compression = 37.4 + 5.407A - 4 - 88B - 1 - 19C + 1.480D	R-Sq = 89.67% R-Sq(adj) = 79.35% S = 2.397
Split tensile strength = -0.35 + 0.516A + 0.371B + 0.151D	R-Sq = 77.80% R-Sq(adj) = 55.6% S = 0.356775

$$CO_{2-M} = \sum_{i=1}^n (W_i \times CO_{2(i)-LCI}) \tag{6}$$

$$CO_{2-T} = \sum_{i=1}^n (W_i \times D_i \times CO_{2(i)-LCI(TR)}) + D_B \times CO_{2(i)-LCI(TR\ CONS)} \tag{7}$$

where *i* is raw material, *n* is total number of raw material, *W<sub>i</sub>* is unit volume weight (kg/m<sup>3</sup>), *CO<sub>2 (i)-LCI</sub>* is *CO<sub>2</sub>* inventory of the material (CO<sub>2</sub>-kg/kg) of the *i*th material,

*D<sub>i</sub>* is the distance between source material to concrete plant, *CO<sub>2 (i)-LCI(TR)</sub>* is the *CO<sub>2</sub>* inventory of the vehicle. *D<sub>B</sub>* is the distance from the concrete plant to the site. *CO<sub>2 (i)-LCI (TR CONS)</sub>* is the *CO<sub>2</sub>* inventory of the transit mix truck.

In this session, the *CO<sub>2</sub>* emission of GGBS–dolomite geopolymer concrete having a strength of 50 N/mm<sup>2</sup> is compared with normal concrete (Gettu et al. 2019); (Bahrami et al. 2013a); (Bahrami and Kouhi 2020); (Singh et al. 2022); (Bahrami and Yavari 2019); (Bahrami and Matinrad 2019);

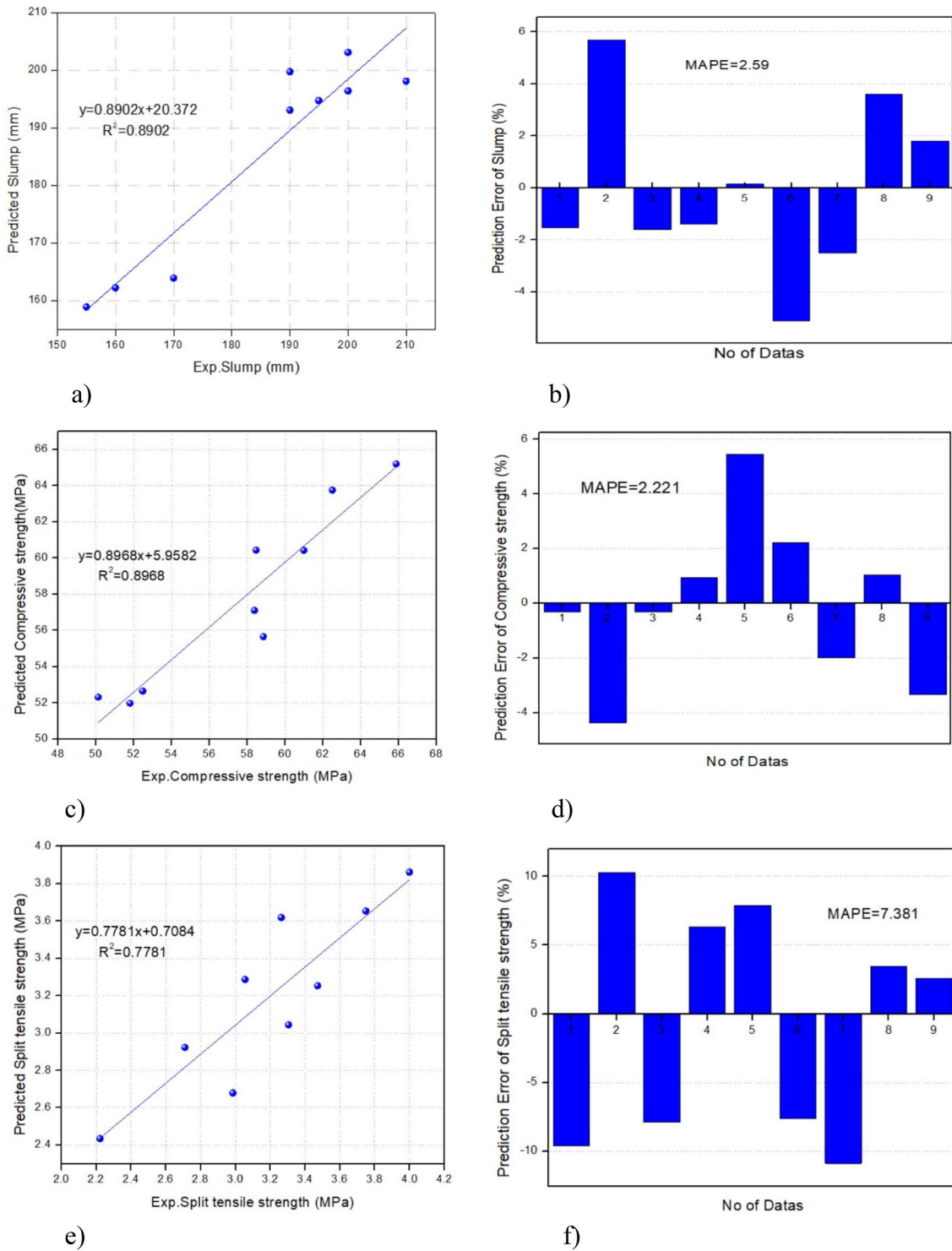


**Fig. 16** a Correlation of pre. slump vs. exp. slump, b prediction error of slump, c correlation of pre. strength in compression vs. exp. strength in compression, d prediction of strength in compression, e

correlation of pre. split tensile strength vs. exp. split tensile strength, f prediction error of split tensile strength

(Bahrami et al. 2021b); (Bahrami et al. 2021a); (Bahrami and Rashid 2023); (Bahrami et al. 2022); (Bahrami et al. 2013b) and fly ash-based geopolymer concrete (Pachamuthu

and Thangaraju 2017) from the literature having the same strength. The CO<sub>2</sub> assessment of normal concrete, fly ash-based geopolymer concrete, and GGBS–dolomite

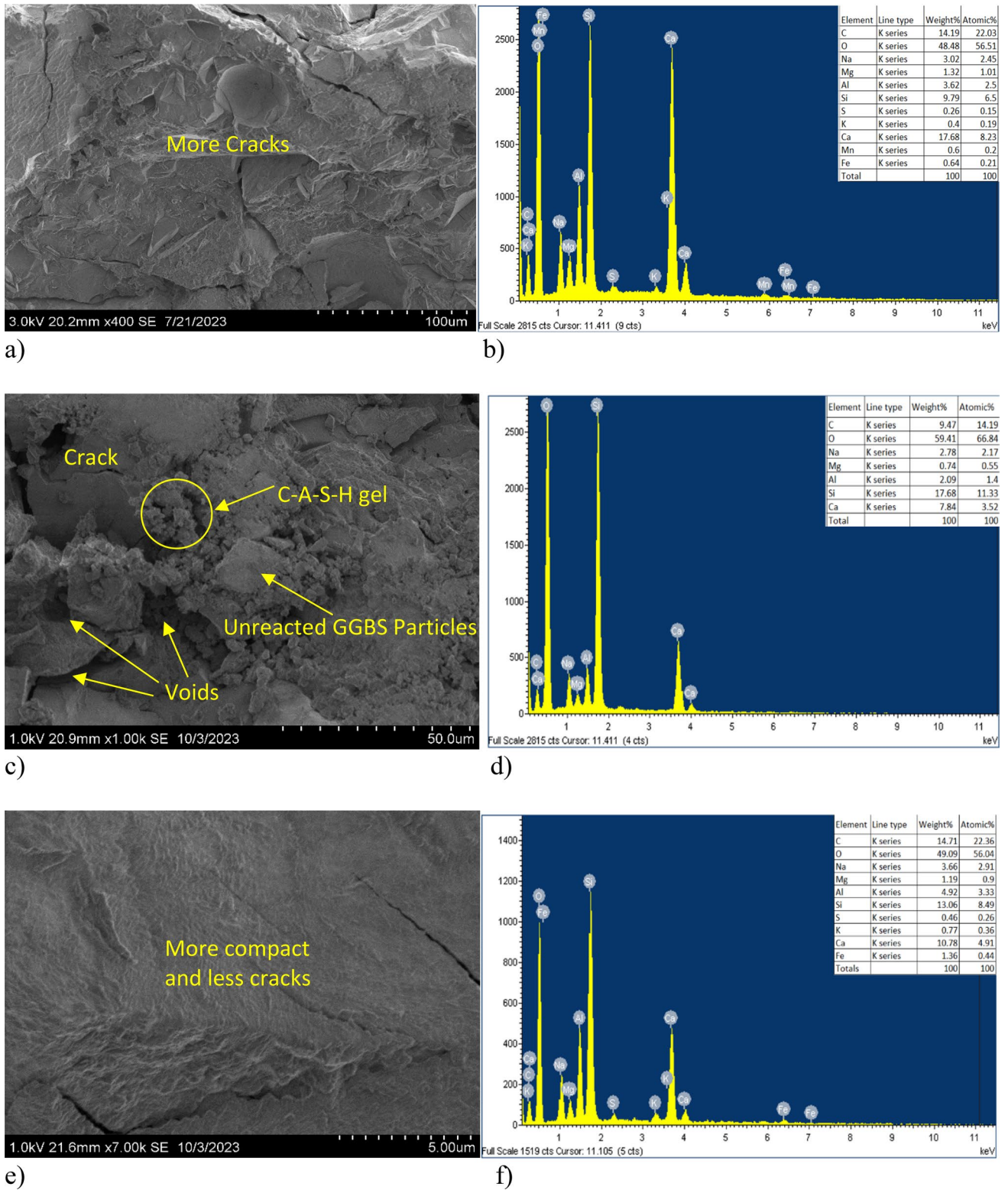


**Fig. 17** a SEM of Mix G70:D30, b EDX of Mix G70:D30, c SEM of Mix G80:D20, d EDX of Mix G80:D20, e SEM of Mix G90:D10, f EDX of Mix G90:D10

**Table 14** Percentage of elements by EDX analysis (%Weight)

Element	Si K	O K	Na K	Ca K	Al K	Si/Al
G70:D30	9.79	48.48	3.02	17.68	3.62	2.70
G80:D20	17.68	59.41	2.78	7.84	2.09	8.46
G90:D10	13.06	49.09	3.66	10.78	4.92	2.65

**Table 15** CO<sub>2</sub> assessment of normal concrete having compressive strength of 50 N/mm<sup>2</sup>

CO <sub>2</sub> assessment of normal concrete having compressive strength of 50N/mm <sup>2</sup>							Total
Functional Unit(FU): m <sup>3</sup>	Material production				Transportation		Total
	A	B	A.B	D	E	A.D.E	
Item	kg/FU	CO <sub>2</sub> -kg/kg	CO <sub>2</sub> -kg/FU	km	CO <sub>2</sub> -kg/kg km	CO <sub>2</sub> -kg/FU	
OPC	360	0.9440	339.8400	100	0.0000518	1.8648	341.70
Fine aggregate	703	0.0026	1.8278	50	0.000063	2.21445	4.04
Coarse aggregate	1193	0.0075	8.9475	50	0.000063	3.75795	12.71
Water	144	0.0002	0.0282	0		0	0.03
Concrete Production	2369.8	0.0080	18.9584	30	0.674	20.22 (D.E)	39.18
Total (CO <sub>2</sub> -kg/FU)							397.66

**Table 16** CO<sub>2</sub> assessment of fly ash-based geopolymer concrete having compressive strength of 50 N/mm<sup>2</sup>

CO <sub>2</sub> Assessment of fly ash-based geopolymer concrete having compressive strength of 50 N/mm <sup>2</sup>							Total
Functional Unit(FU): m <sup>3</sup>	Material production				Transportation		Total
	A	B	A.B	D	E	A.D.E	
Item	kg/FU	CO <sub>2</sub> -kg/kg	CO <sub>2</sub> -kg/FU	km	CO <sub>2</sub> -kg/kg km	CO <sub>2</sub> -kg/FU	
Fly ash	425.75	0.0196	8.34	100	0.0000518	2.21	10.55
Fine aggregate	642.51	0.0026	1.67	50	0.0000630	2.02	3.69
Coarse aggregate	1212.6	0.0075	9.09	50	0.0000630	3.82	12.91
NaOH	54.74	1.2320	67.44	30	0.0002210	0.36	67.80
Na <sub>2</sub> SiO <sub>3</sub>	136.84	1.3200	180.63	30	0.0002210	0.91	181.54
Concrete production	2708.40	0.0080	21.67	30	0.0000518	0.001554	21.001
Steam curing (85 °C/24 h: 38.5 CO <sub>2</sub> -kg/FU)							38.5
Total (CO <sub>2</sub> -kg/FU)							335.99

**Table 17** CO<sub>2</sub> assessment of GGBS–dolomite geopolymer concrete having compressive strength of 50N/mm<sup>2</sup>

CO <sub>2</sub> assessment of GGBS–dolomite geopolymer concrete having compressive strength of 50 N/mm <sup>2</sup>							Total
Functional Unit(FU): m <sup>3</sup>	Material production				Transportation		Total
	A	B	A.B	D	E	A.D.E	
Item	kg/FU	CO <sub>2</sub> -kg/kg	CO <sub>2</sub> -kg/FU	km	CO <sub>2</sub> -kg/kg km	CO <sub>2</sub> -kg/FU	
GGBS	298.71	0.0265	7.915	100	0.0000518	1.547	9.462
Dolomite	128.02	0.0075	0.960	100	0.0000518	0.663	1.623
Fine aggregate	757.36	0.0026	1.969	50	0.0000630	2.385	4.354
Coarse aggregate	976	0.0075	7.320	50	0.0000630	3.074	10.394
NaOH	60.96	1.2320	75.102	30	0.0002210	0.404	75.506
Na <sub>2</sub> SiO <sub>3</sub>	152.41	1.3200	201.181	30	0.0002210	1.010	202.191
Concrete Production	2708.40	0.0080	21.667	30	0.0000518	0.001554	21.668
Total(CO <sub>2</sub> -kg/FU)							325.198

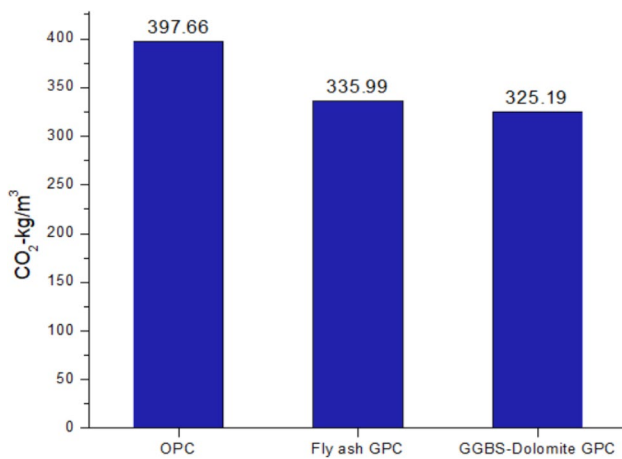


**Fig. 18** CO<sub>2</sub> emission comparison

geopolymer concrete is shown in Tables 15, 16, and 17, respectively. In the analysis, it is assumed that the binder is transported from 100 km distance, whereas the aggregates from 50 km and the distance between concrete plant and site is 30 km. The oven-curing is necessary for fly ash; hence, 38.5 CO<sub>2</sub>-kg/m<sup>3</sup> is considered for it.

The data presented in Tables 15, 16, and 17 indicate that the CO<sub>2</sub> emissions from 50 N/mm<sup>2</sup> GGBS–dolomite geopolymer concrete are less than those emitted by normal concrete of the same grade and geopolymer concrete based on fly ash. In comparison with normal concrete, fly ash-based geopolymer demonstrates a 15.55% reduction in CO<sub>2</sub> emissions, whereas GGBS–dolomite geopolymer concrete exhibits an even greater reduction of 18.22%.

Figure 18 depicts the comparison of CO<sub>2</sub> emission of normal concrete, fly ash GPC, and GGBS–dolomite GPC. Generally, geopolymer concrete tends to result in reduced CO<sub>2</sub> emissions when compared to conventional normal concrete, thereby providing societal environmental benefits.

## 9 Conclusions

In this study, the design variables in a geopolymer concrete are optimized using the Taguchi method. The analysis and experimental evaluation led to the following conclusion.

- Obtaining higher compressive strength requires an optimal mixture of materials, including superplasticizer dosage of 1.25%, Na<sub>2</sub>SiO<sub>3</sub>/NaOH ratio of 1.5, and 14 M NaOH (binder proportion B3). It is important to note that the same binder proportion yields an enhanced value for split tensile strength.
- The mix design process developed for a target strength of 45 MPa demonstrated a strong correlation with the

experimental assessment of the GPC specimens, in accordance with the IS: 10,262–2019 standards.

- The Taguchi L9 OA was deemed appropriate for identifying the optimal mixture of constituents, avoiding undesired trial mixes to achieve the target strength. However, for future research, it is recommended to incorporate additional mix design parameters with varying levels for a specific GPC mix design strength.
- The current investigation underscored the significance of mix design parameters in the optimization process, particularly the proportion of binder, the dosage of superplasticizer, Na<sub>2</sub>SiO<sub>3</sub>/NaOH ratio, and the molarity of the NaOH solution, in achieving the desired strength in accordance with standard design steps.
- ANOVA results highlighted that when considering GGBS–dolomite GPC, the main factor influencing compression strength and split tensile strength was the binder proportion. On the other hand, the Na<sub>2</sub>SiO<sub>3</sub>/NaOH ratio and superplasticizer dosage showed negligible effects, allowing for the production of concrete with high strength levels above 50 MPa regardless of changes in these parameters.
- The predictive outcomes revealed that the average prediction errors (MAPEs) for compressive strength, workability, and split tensile strength were notably low. This suggests that these prediction models can be effectively employed to estimate the required properties.
- The compressive strength testing results are substantially consistent with the SEM/EDX results. According to analysis, the compactness of the geopolymer concrete improved with a larger GGBS content, whereas the structure was less dense with a lower GGBS percentage.
- GGBS–dolomite geopolymer concrete consistently exhibited a substantial reduction of 18.22% in CO<sub>2</sub> emissions in comparison with equivalent-grade conventional concrete and 15.55% less than that of same-grade fly ash-based geopolymer concrete, establishing it as an eco-friendly and sustainable construction material.

## References

- Ahmad Dar T, Azam F (2015) Development of fly ash based geopolymer concrete. *Int J Sci Res* 6:1539–1560
- Alexander AE, Shashikala AP (2022) Studies on the microstructure and durability characteristics of ambient cured FA-GGBS based geopolymer mortar. *Constr Build Mater* 347:128538. <https://doi.org/10.1016/j.conbuildmat.2022.128538>
- Al-majidi MH, Lampropoulos A, Cundy AB (2017) Steel fibre reinforced geopolymer concrete (SFRGC) with improved microstructure and enhanced fibre-matrix interfacial properties. *Constr Build*

- Mater 139:286–307. <https://doi.org/10.1016/j.conbuildmat.2017.02.045>
- Arthur S, Saitoh M, Pal SK (2020) Lecture Notes in Civil Engineering Advances in Civil Engineering
- Bahrami A, Kouhi AM (2020) Compressive behaviour of circular, square, and rectangular concrete-filled steel tube stub columns. *Civ Eng Archit* 8:1119–1126. <https://doi.org/10.13189/cea.2020.080538>
- Bahrami A, Matinrad S (2019) Response of steel beam-to-column bolted connections to blast loading. *Int J Recent Technol Eng* 8:3639–3648. <https://doi.org/10.35940/ijrte.C5347.098319>
- Bahrami A, Rashid SMP (2023) A state-of-the-art review on axial compressive behavior of concrete-filled steel tubes incorporating steel fiber and GFRP jacketing. *Buildings* 13:729
- Bahrami A, Yavari M (2019) Hysteretic assessment of steel-concrete composite shear walls. *Int J Recent Technol Eng* 8:5640–5645. <https://doi.org/10.35940/ijrte.B2302.078219>
- Bahrami A, Wan Badaruzzaman WH, Osman SA (2013a) Performance of axially loaded tapered concrete-filled steel composite slender columns. *J Civ Eng Manag* 19:705–717. <https://doi.org/10.3846/13923730.2013.799094>
- Bahrami A, Wan Badaruzzaman WH, Osman SA (2013b) Investigation of concrete-filled steel composite (CFSC) stub columns with bar stiffeners. *J Civ Eng Manag* 19:433–446. <https://doi.org/10.3846/13923730.2013.768545>
- Bahrami A, Nexén O, Jonsson J (2021a) Comparing performance of cross-laminated timber and reinforced concrete walls. *Int J Appl Mech Eng* 26:28–43. <https://doi.org/10.2478/ijame-2021-0033>
- Bahrami A, Vall A, Khalaf A (2021b) Comparison of cross-laminated timber and reinforced concrete floors with regard to load-bearing properties. *Civ Eng Archit* 9:1395–1408. <https://doi.org/10.13189/CEA.2021.090513>
- Bahrami A, Deniz S, Moalin H (2022) Vertical extension of a multi-storey reinforced concrete building. *Int J Appl Mech Eng* 27:1–20. <https://doi.org/10.2478/ijame-2022-0001>
- Barbhuiya S (2011) Effects of fly ash and dolomite powder on the properties of self-compacting concrete. *Constr Build Mater* 25:3301–3305. <https://doi.org/10.1016/j.conbuildmat.2011.03.018>
- Cao YF, Tao Z, Pan Z, Wuhrer R (2018) Effect of calcium aluminate cement on geopolymer concrete cured at ambient temperature. *Constr Build Mater* 191:242–252. <https://doi.org/10.1016/j.conbuildmat.2018.09.204>
- Dave SV, Bhogayata A (2020) The strength oriented mix design for geopolymer concrete using Taguchi method and Indian concrete mix design code. *Constr Build Mater* 262:120853. <https://doi.org/10.1016/j.conbuildmat.2020.120853>
- Dave SV, Bhogayata A, Arora NK (2021) Mix design optimization for fresh, strength and durability properties of ambient cured alkali activated composite by Taguchi method. *Constr Build Mater* 284:122822. <https://doi.org/10.1016/j.conbuildmat.2021.122822>
- Davidovits J (1989) Geopolymers and geopolymeric materials. *J Therm Anal* 35:429–441
- De Silva P, Sagoe-Crenstil K, Sirivivatnanon V (2007) Kinetics of geopolymerization: role of  $Al_2O_3$  and  $SiO_2$ . *Cem Concr Res* 37:512–518. <https://doi.org/10.1016/j.cemconres.2007.01.003>
- Deb PS, Nath P, Sarker PK (2014) The effects of ground granulated blast-furnace slag blending with fly ash and activator content on the workability and strength properties of geopolymer concrete cured at ambient temperature. *J Mater* 62:32–39. <https://doi.org/10.1016/j.matdes.2014.05.001>
- Deb PS, Nath P, Sarker PK (2015) Drying shrinkage of slag blended fly ash geopolymer concrete cured at room temperature. *Procedia Eng* 125:594–600. <https://doi.org/10.1016/j.proeng.2015.11.066>
- Detphan S, Chindapasirt P (2009) Preparation of fly ash and rice husk ash geopolymer. *Int J Miner Metall Mater* 16:720–726. [https://doi.org/10.1016/S1674-4799\(10\)60019-2](https://doi.org/10.1016/S1674-4799(10)60019-2)
- Duxson P, Mallicoat SW, Lukey GC et al (2007) The effect of alkali and Si/Al ratio on the development of mechanical properties of metakaolin-based geopolymers. *Colloids Surfaces A Physicochem Eng Asp* 292:8–20. <https://doi.org/10.1016/j.colsurfa.2006.05.044>
- Ferdous MW, Kayali O, Khennane A (2013) A detailed procedure of mix design for fly ash based geopolymer concrete. In: *Proceedings 4th Asia-Pacific Conf FRP Struct APFIS 2013* pp. 11–13
- Fernández-Jiménez A, Palomo A, Criado M (2005) Microstructure development of alkali-activated fly ash cement: a descriptive model. *Cem Concr Res* 35:1204–1209. <https://doi.org/10.1016/j.cemconres.2004.08.021>
- Galí S, Ayora C, Alfonso P et al (2001) Kinetics of dolomite-portlandite reaction—Application to portland cement concrete. *Cem Concr Res* 31:933–939. [https://doi.org/10.1016/S0008-8846\(01\)00499-9](https://doi.org/10.1016/S0008-8846(01)00499-9)
- García-Lodeiro I, Fernández-Jiménez A, Palomo A (2013) Variation in hybrid cements over time. Alkaline activation of fly ash-portland cement blends. *Cem Concr Res* 52:112–122. <https://doi.org/10.1016/j.cemconres.2013.03.022>
- García-Lodeiro I, Donatello S, Fernández-Jiménez A, Palomo A (2016) Hydration of hybrid alkaline cement containing a very large proportion of fly ash: a descriptive model. *Materials* 9:605. <https://doi.org/10.3390/MA9070605>
- Gettu R, Patel A, Rathi V et al (2019) Influence of supplementary cementitious materials on the sustainability parameters of cements and concretes in the Indian context. *Mater Struct Constr* 52:1–11. <https://doi.org/10.1617/s11527-019-1321-5>
- Guo X, Shi H, Chen L, Dick WA (2010) Alkali-activated complex binders from class C fly ash and Ca-containing admixtures. *J Hazard Mater* 173:480–486. <https://doi.org/10.1016/j.jhazmat.2009.08.110>
- Hadi MNS, Farhan NA, Sheikh MN (2017) Design of geopolymer concrete with GGBFS at ambient curing condition using Taguchi method. *Constr Build Mater* 140:424–431. <https://doi.org/10.1016/j.conbuildmat.2017.02.131>
- Hadi MNS, Zhang H, Parkinson S (2019) Optimum mix design of geopolymer pastes and concretes cured in ambient condition based on compressive strength, setting time and workability. *J Build Eng* 23:301–313. <https://doi.org/10.1016/j.jobbe.2019.02.006>
- Jithendra C, Elavenil S (2020) Influences of parameters on slump flow and compressive strength properties of aluminosilicate based flowable geopolymer concrete using Taguchi method. *SILICON* 12:595–602. <https://doi.org/10.1007/s12633-019-00166-w>
- Khale D, Chaudhary R (2007) Mechanism of geopolymerization and factors influencing its development: a review. *J Mater Sci* 42:729–746
- Lee NK, Jang JG, Lee HK (2014) Shrinkage characteristics of alkali-activated fly ash/slag paste and mortar at early ages. *Cem Concr Compos* 53:239–248. <https://doi.org/10.1016/j.cemconcomp.2014.07.007>
- Lekshmi S, Sudhakumar J (2022) An assessment on the durability performance of fly ash-clay based geopolymer mortar containing clay enhanced with lime and GGBS. *Clean Mater* 5:100129. <https://doi.org/10.1016/j.clema.2022.100129>
- Lekshmi S, Sudhakumar J (2022) Performance of fly ash geopolymer mortar containing clay blends. *ACI Mater J* 119(4):15–26. <https://doi.org/10.14359/51734682>
- Li N, Shi C, Zhang Z et al (2019) A review on mixture design methods for geopolymer concrete. *Compos Part B Eng* 178:107490. <https://doi.org/10.1016/j.compositesb.2019.107490>
- Mareya M, Bahurudeen A, Varghese J et al (2023) Transformation of rice husk modified basic oxygen furnace slag into geopolymer

- composites. *J Mater Res Technol* 24:6264–6278. <https://doi.org/10.1016/j.jmrt.2023.04.225>
- Marín-López C, Reyes Araiza JL, Manzano-Ramírez A et al (2009) Synthesis and characterization of a concrete based on metakaolin geopolymer. *Inorg Mater* 45:1429–1432. <https://doi.org/10.1134/S0020168509120231>
- Mathew G, Issac BM (2020) Effect of molarity of sodium hydroxide on the aluminosilicate content in laterite aggregate of laterised geopolymer concrete. *J Build Eng* 32:101486. <https://doi.org/10.1016/j.jobe.2020.101486>
- Nakkeeran G, Krishnaraj L, Bahrami A et al (2023) Machine learning application to predict the mechanical properties of Glass Fiber mortar. *Adv Eng Softw* 180:103454. <https://doi.org/10.1016/j.advengsoft.2023.103454>
- Nath P, Sarker PK (2014) Effect of GGBFS on setting, workability and early strength properties of fly ash geopolymer concrete cured in ambient condition. *Constr Build Mater* 66:163–171. <https://doi.org/10.1016/j.conbuildmat.2014.05.080>
- Nazar S, Yang J, Ahmad A, Shah SFA (2022) Comparative study of evolutionary artificial intelligence approaches to predict the rheological properties of fresh concrete. *Mater Today Commun* 32:103964. <https://doi.org/10.1016/j.mtcomm.2022.103964>
- Nazar S, Yang J, Amin MN et al (2023a) Formulation of estimation models for the compressive strength of concrete mixed with nanosilica and carbon nanotubes. *Dev Built Environ* 13:100113. <https://doi.org/10.1016/j.dibe.2022.100113>
- Nazar S, Yang J, Amin MN et al (2023b) Investigating the influence of PVA and PP fibers on the mechanical, durability, and microstructural properties of one-part alkali-activated mortar: An experimental study. *J Mater Res Technol* 25:3482–3495. <https://doi.org/10.1016/j.jmrt.2023.06.115>
- Nazar S, Yang J, Amin MN et al (2023c) Machine learning interpretable-prediction models to evaluate the slump and strength of fly ash-based geopolymer. *J Mater Res Technol* 24:100–124. <https://doi.org/10.1016/j.jmrt.2023.02.180>
- Nazar S, Yang J, Ashraf M et al (2023d) Formulation and characterization of cleaner one-part novel fly ash/lime-based alkali-activated material. *J Mater Res Technol* 23:3821–3839. <https://doi.org/10.1016/j.jmrt.2023.02.022>
- Nazar S, Yang J, Faisal Javed M et al (2023e) An evolutionary machine learning-based model to estimate the rheological parameters of fresh concrete. *Structures* 48:1670–1683. <https://doi.org/10.1016/j.istruc.2023.01.019>
- Nazar S, Yang J, Khan MS et al (2023f) Investigating the effects of MWCNTs on sustainable alkali-activated mortar: physical, rheological, and mechanical analysis. *Mater Today Sustain* 24:100519. <https://doi.org/10.1016/j.mtsust.2023.100519>
- Nazar S, Yang J, Wang XE et al (2023g) Estimation of strength, rheological parameters, and impact of raw constituents of alkali-activated mortar using machine learning and SHapely Additive exPlanations (SHAP). *Constr Build Mater* 377:131014. <https://doi.org/10.1016/j.conbuildmat.2023.131014>
- Nazari A, Khanmohammadi H, Amini M et al (2012) Production geopolymers by Portland cement: designing the main parameters' effects on compressive strength by Taguchi method. *Mater Des* 41:43–49. <https://doi.org/10.1016/j.matdes.2012.04.045>
- Obeng J, Andrews A, Adom-Asamoah M, Adjei S (2023) Effect of calcium carbide residue on the sulphate resistance of metakaolin-based geopolymer mortars. *Clean Mater* 7:100177. <https://doi.org/10.1016/j.clema.2023.100177>
- Onya ME, Ikeagwuani CC, Egbo MC (2022) Effect of pressed palm oil fruit fibre on mechanical properties of sandcrete masonry blocks using Taguchi-grey relational analysis optimization technique. *Clean Mater* 5:100124. <https://doi.org/10.1016/j.clema.2022.100124>
- Pachamuthu S, Thangaraju P (2017) Utjecaj pepela iz papirnog mulja na geopolimerni beton s letećim pepelom. *Gradjevinar* 69:851–859. <https://doi.org/10.14256/JCE.1864.2016>
- Pavithra P, Srinivasula Reddy M, Dinakar P et al (2016) A mix design procedure for geopolymer concrete with fly ash. *J Clean Prod* 133:117–125. <https://doi.org/10.1016/j.jclepro.2016.05.041>
- Rattanasak U, Chindaprasirt P (2009) Influence of NaOH solution on the synthesis of fly ash geopolymer. *Miner Eng* 22:1073–1078. <https://doi.org/10.1016/j.mineng.2009.03.022>
- Sajan P, Jiang T, Lau CK et al (2021) Combined effect of curing temperature, curing period and alkaline concentration on the mechanical properties of fly ash-based geopolymer. *Clean Mater* 1:0002. <https://doi.org/10.1016/j.clema.2021.100002>
- Salih MA, Farzadnia N, Abang Ali AA, Demirboga R (2015) Development of high strength alkali activated binder using palm oil fuel ash and GGBS at ambient temperature. *Constr Build Mater* 93:289–300. <https://doi.org/10.1016/j.conbuildmat.2015.05.119>
- Saranya P, Nagarajan P, Shashikala AP (2019a) Development of ground-granulated blast-furnace slag-dolomite geopolymer concrete. *ACI Mater J* 116:235–243. <https://doi.org/10.14359/51716981>
- Saranya P, Nagarajan P, Shashikala AP (2019b) Performance evaluation of geopolymer concrete beams under monotonic loading performance evaluation of geopolymer concrete beams under monotonic loading. *Structures*. <https://doi.org/10.1016/j.istruc.2019.06.010>
- Saranya P, Nagarajan P, Shashikala AP (2020) Journal of building engineering behaviour of GGBS—dolomite geopolymer concrete short column under axial loading. *J Build Eng* 30:101232. <https://doi.org/10.1016/j.jobe.2020.101232>
- Saranya P, Nagarajan P, Shashikala AP (2021) Performance studies on steel fiber—reinforced GGBS-dolomite geopolymer concrete. *J Mater Civil Eng*. 33:1–8. [https://doi.org/10.1061/\(ASCE\)MT.1943-5533.0003530](https://doi.org/10.1061/(ASCE)MT.1943-5533.0003530)
- Shi C, Jiménez AF, Palomo A (2011) New cements for the 21st century: the pursuit of an alternative to Portland cement. *Cem Concr Res* 41:750–763. <https://doi.org/10.1016/j.cemconres.2011.03.016>
- Singh R, Arora HC, Bahrami A et al (2022) Enhancing sustainability of corroded RC structures: estimating steel-to-concrete bond strength with ANN and SVM algorithms. *Materials* 15:8295. <https://doi.org/10.3390/ma15238295>
- Skariah Thomas B, Yang J, Bahurudeen A et al (2022) Geopolymer concrete incorporating recycled aggregates: a comprehensive review. *Clean Mater* 3:100056. <https://doi.org/10.1016/j.clema.2022.100056>
- Türkmen İ, Gül R, Çelik C, Demirboğa R (2003) Determination by the taguchi method of optimum conditions for mechanical properties of high strength concrete with admixtures of silica fume and blast furnace slag. *Civ Eng Environ Syst* 20:105–118. <https://doi.org/10.1080/1028660031000081527>
- Türkmen I, Gül R, Çelik C (2008) A Taguchi approach for investigation of some physical properties of concrete produced from mineral admixtures. *Build Environ* 43:1127–1137. <https://doi.org/10.1016/j.buildenv.2007.02.005>
- Unis Ahmed H, Mahmood LJ, Muhammad MA et al (2022) Geopolymer concrete as a cleaner construction material: an overview on

- materials and structural performances. *Clean Mater* 5:100111. <https://doi.org/10.1016/j.clema.2022.100111>
- Yang KH, Song JK, Il SK (2013) Assessment of CO<sub>2</sub> reduction of alkali-activated concrete. *J Clean Prod* 39:265–272. <https://doi.org/10.1016/j.jclepro.2012.08.001>
- Yip CK, Provis JL, Lukey GC, van Deventer JSJ (2008) Carbonate mineral addition to metakaolin-based geopolymers. *Cem Concr Compos* 30:979–985. <https://doi.org/10.1016/j.cemconcomp.2008.07.004>
- Zheng X, Xie Y, Yang X et al (2023) A data-driven approach to predict the compressive strength of alkali-activated materials and correlation of influencing parameters using SHapley Additive exPlanations (SHAP) analysis. *J Mater Res Technol* 25:4074–4093. <https://doi.org/10.1016/j.jmrt.2023.06.207>

Springer Nature or its licensor (e.g. a society or other partner) holds exclusive rights to this article under a publishing agreement with the author(s) or other rightsholder(s); author self-archiving of the accepted manuscript version of this article is solely governed by the terms of such publishing agreement and applicable law.